LBL-14246
UC-94e

Lawrence Berkeley Laboratory
UNIVERSITY OF CALIFORNIA

EARTH SCIENCES DIVISION

HEAT STORAGE IN AQUIFERS: BUOYANCY FLOW AND THERMAL-STRATIFICATION PROBLEMS

Göran Hellström, Chin Fu Tsang, and Johan Claesson

October 1979

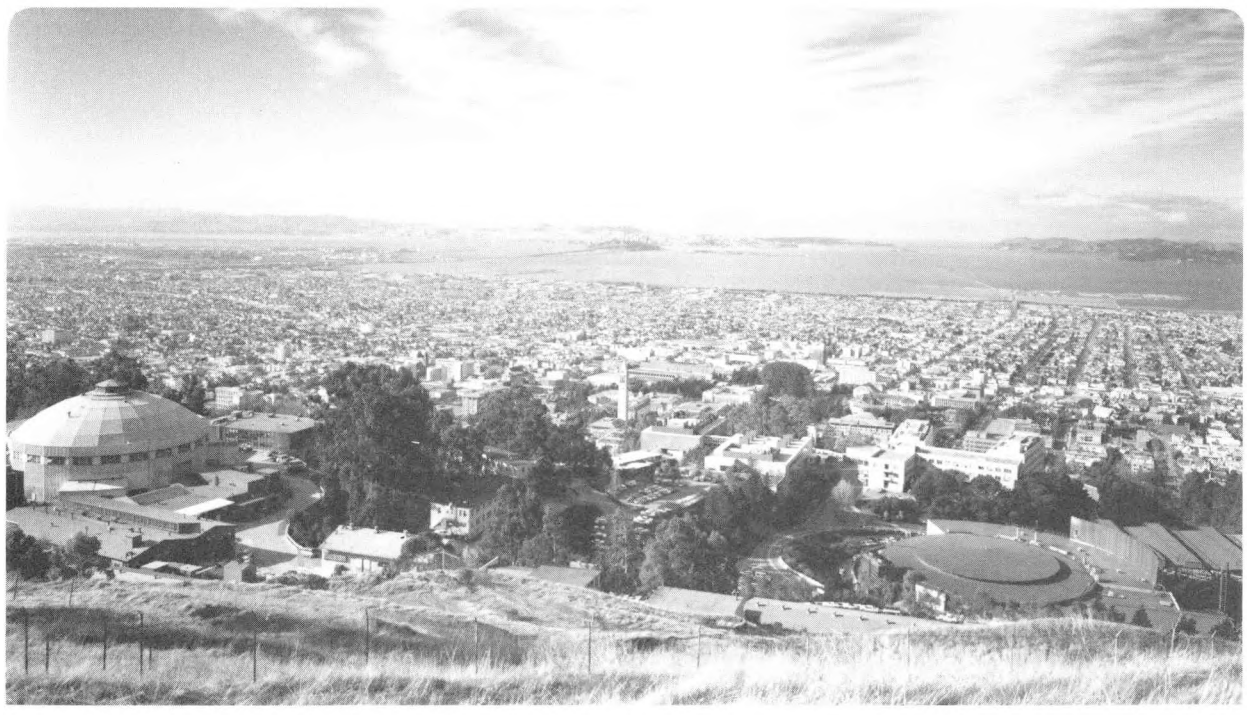

Prepared for the U.S. Department of Energy under Contract DE-AC03-76SF00098

LBL-14246
UC-94e

HEAT STORAGE IN AQUIFERS:

BUOYANCY FLOW AND THERMAL-STRATIFICATION PROBLEMS

Göran Hellström*†, Chin Fu Tsang†, and Johan Claesson*

* Department of Mathematical Physics
Lund Institute of Technology
P. O. Box 725, S-220 07 Lung 7, Sweden

† Earth Sciences Division
Lawrence Berkeley Laboratory
University of California
Berkeley, California 94720

LBL--14246

DE82 013881

October 1979

This work has, from the Swedish side, been supported by the Swedish Council for Building Research and the National Swedish Board for Energy Source Development. In the United States, this work was supported by the Assistant Secretary for Conservation and Solar Energy, Office of Advanced Conservation Technology, Division of Thermal and Mechanical Storage Systems of the U. S. Department of Energy under Contract De-AC03-76SF00098, and was performed within the Seasonal Thermal Energy Storage Program managed by Pacific Northwest Laboratory.

Contents

Introduction

The possibility to store heat in aquifers has attracted considerable attention during the last years. The goal is to be able to store large amounts of heat at moderate temperatures from summer to winter at an acceptable cost. The idea is to inject warm water in a confined aquifer and at a later time recover the heat by pumping back the warm water.

Several solutions have been proposed. One possibility is to have a single well down to a horizontal aquifer stratum. The water is pumped radially outwards and inwards from the well. Other solutions use a two-well system [1].

Aquifers with high permeability are attractive from the point of view that they will require little pumping work. An example of this type is shallow glacio-alluvial aquifers, called eskers, which are common in Sweden. Their suitability for thermal heat storage is under investigation [2]. This study is done in cooperation with that project.

The mentioned systems with vertical bore holes that penetrate the whole aquifer depth have a horizontal injection and extraction of water. The thermal front between injected warm water and colder surrounding regions is primarily vertical. The problem is that such a thermal front is unstable because of the lower density of the warmer water. The thermal front will tilt so that the warmer water eventually ends on top. This and other thermal stratification effects, which entail undesired heat losses, require both theoretical and experimental investigations. Systems that use horizontal injection-extraction devices along the top and bottom of the aquifer region do not have the same stratification problems. The water flow is basically vertical with warmer regions always on top. These injection-extraction systems are however more complicated and expensive.

The heat loss in the aquifer is roughly proportional to the area of the warm storage region. This region shall therefore be kept as compact as possible. Buoyancy effects may increase the surface to an unacceptable degree. Consider for example a horizontal injection of warm water as shown in figure 1. A strong buoyancy flow will concentrate the injected warm water in only the upper part of the aquifer. The warm region

($T=T_1$) will look like a thin tongue, which protrudes into the cold regions ($T=T_0$). The heat losses become excessive, and the system cannot be used. The lower viscosity of warmer water aggravates the stratification during the loading phase.

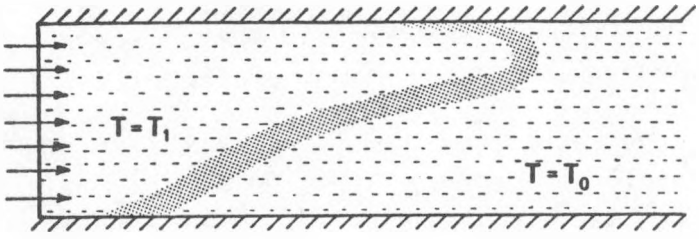

Figure 1. Horizontal injection of warmer water in an aquifer with excessive thermal stratification.

It is necessary to be able to predict the buoyancy flow and the tilting rate of a more or less vertical thermal front for pertinent situations in different aquifer types. This paper discusses these thermohydraulic problems in heat storage aquifers. Some general observations are made. Results of some analytical solutions are presented. The superposition of forced and natural convection is dealt with. Formulas for the tilting of the thermal front as a function of time are given. These are tested against numerical simulations and applied to laboratory and field experiments. The different results, formulas, and tilting criteria are summarized in the last paragraph.

Thermohydraulic equations

The coupled ground water and heat flow process in the aquifer is governed by two partial differential equations. The volumetric ground water flow $\bar{q}$ is related to the pressure gradient and the gravity force through the empirical law of Darcy:

$$\bar{q} = -\frac{k}{\mu}(\nabla P + \rho g \hat{z}). \qquad (1)$$

The permeability is k. The water density ρ and the viscosity μ are functions of the temperature.

The above formula assumes anisotropic aquifer. We will below also study cases, when the aquifer has different permeabilities in the horizontal (x,y) and vertical (z) directions. Then we have

$$q_x = -\frac{k}{\mu}\frac{\partial P}{\partial x} \qquad q_y = -\frac{k}{\mu}\frac{\partial P}{\partial y} \qquad q_z = -\frac{k'}{\mu}\left(\frac{\partial P}{\partial z} + \rho g\right) \tag{2}$$

The permeability in the vertical direction is denoted k'.

Compressibility effects are neglected in this study. The divergence of the ground water flow $\bar{q}$ is then zero at each point:

$$\nabla \cdot \bar{q} = \nabla \cdot \left[-\frac{k}{\mu}(\nabla P + \rho g \hat{z})\right] = 0 \tag{3}$$

The temperature shall satisfy the equation

$$C\frac{\partial T}{\partial t} = \nabla \cdot (\lambda \nabla T - TC_w \bar{q}) \tag{4}$$

Here C and C_w are the volumetric heat capacities for aquifer (matrix plus water) and water respectively. The thermal conductivity λ includes a contribution from the ground water dispersion.

The convective heat flow is given by $TC_w \bar{q}$. The thermal velocity is

$$\bar{v}_T = \frac{C_w}{C}\bar{q} \tag{5}$$

The thermal velocity represents the convective displacement of the temperature field. The total change of the temperature field is, at each time, a superposition of the convective displacement and a heat diffusion.

The aquifer region is bounded by impermeable layers and injection/extraction wells. At an impermeable boundary the perpendicular ground water flow component vanishes. The boundary conditions at the wells are determined by the mode of operation of the well. The temperature of injected water is given. Outside the aquifer region the ordinary heat flow equation prevails.

The pressure distribution and the ground water flow pattern are coupled to the temperature field through the density $\rho(T)$ and viscosity $\mu(T)$. At each time there is a certain temperature distribution through the aquifer. This temperature distribution and the boundary conditions at the wells determine the ground water flow. The temperature changes with time due to the convective and diffusive heat flows. The ground water flow pattern will gradually change with time due to the changed densities $\rho(T)$ and viscosities $\mu(T)$ throughout the aquifer.

The ground water flow at a given time is thus determined by the actual temperature field and the conditions at the wells. During storage periods without injection and extraction there is a pure buoyancy flow, which is caused by density variations of the water in the aquifer . The perpendicular ground water flow shall vanish at all boundaries. During injection and extraction periods there is a forced convection due to the pumping. The natural convection due to buoyancy is superimposed on the forced convection.

The major concern in this paper is the motion of thermal fronts in an aquifer which is used for heat storage. The thermal front between the warm region and colder surrounding regions may be more or less sharp and well-defined. The front is displaced by the thermal velocity field $\bar{v}_T$. Heat diffusion will simultaneously widen the thermal front.

The motion of a thermal front is determined by the flow velocity $\bar{v}_T$ or $\bar{q}$ at the front. The flow $\bar{q}$ is determined by the temperature distribution, which in turn essentially is given by the position of the thermal front. We want to learn how the thermal front moves in various situations. Our task is then to determine the ground water flow for various, pertinent positions of a thermal front in the aquifer.

There are two cases. The simpler situation is that of pure buoyancy flow during rest periods without injection and extraction of water. Then there is the more complex case of combined buoyancy flow and forced convection during loading and extraction periods.

We will first discuss the simpler case of pure buoyancy flow and then the case of combined forced and natural convection. These discussions concern only the momentary ground water flow at a given time. The complete thermohydraulic process is simulated by the numerical computer code CCC developed at LBL.

Buoyancy flow

The temperature field in the heat storage aquifer gives a variable water density and an ensuing buoyancy flow in the aquifer. We will in particular consider the situation, when the aquifer may be separated into a warm region ($T=T_1$) and a cold region ($T=T_0$). These regions are separated by a thermal front zone, through which the temperature falls from T_1 to T_0. The idealization of an infinitely thin or sharp thermal front will also be considered. This is often a quite reasonable and useful approximation.

The whole boundary is considered impermeable during periods of pure buoyancy flow (no injection/extraction). The ground water flow shall tend to zero in free regions that extend to infinity.

Figure 2 shows the type of situation that we have in mind. The aquifer occupies a semi-infinite horizontal strip. Warm water has been injected through the left vertical boundary. There is a warmer region with a vertical (A) or tilted (B) thermal front zone.

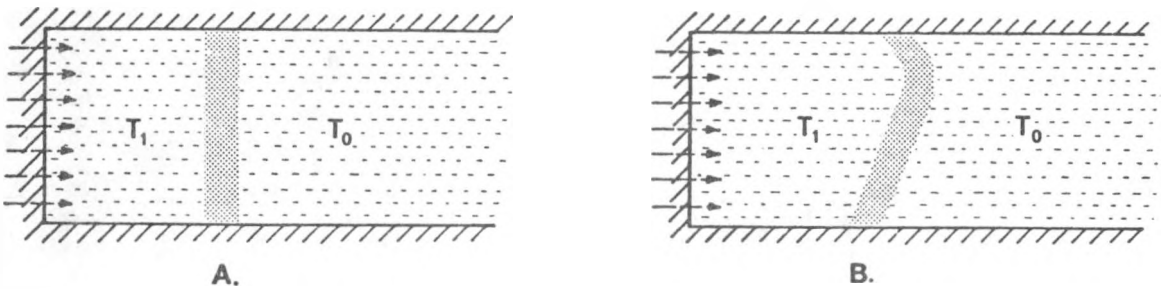

Figure 2. Vertical (A) or tilted (B) thermal front in an aquifer with injection through the left boundary.

Figure 2 applies both to the plane and the cylindrical case. In the latter case there is rotational symmetry around the left vertical boundary, where the bore-hole lies.

The goal is to be able to quantify the motion of the thermal front due to buoyancy flow. It should be remembered that we discuss the momentary flow for a given temperature field at a certain time.

The following observation is useful in order to understand the flow process. Let Γ be any closed curve in the aquifer. The line integral along Γ of the gradient of the pressure is automatically zero. Darcy's relation (1) gives then

$$\int_{\Gamma} \frac{\mu}{k} \bar{q} \cdot d\bar{r} = g\,(-\hat{z}) \cdot \int_{\Gamma} \rho \, d\bar{r} \qquad (6)$$

The right-hand term represents a net driving force due to density variations along Γ. The left-hand side gives an integral of the tangential component of the flow $\bar{q}$ along Γ. The flow is weighted with the flow resistance coefficient $\frac{\mu}{k}$. The right-hand side is known, when the temperature and hence the density field is given. The formula provides some information on the magnitude of the flow velocities.

Figure 3 shows a case when the curve Γ crosses a sharp thermal front. The density and viscosity on the warm and cold sides are denoted ρ_1, μ_1 and ρ_o, μ_o respectively.

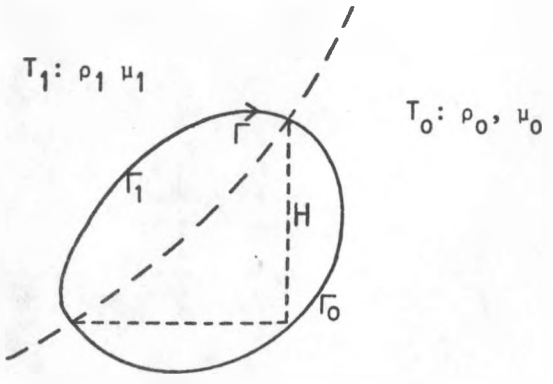

Figure 3. Closed curve Γ in an aquifer with a sharp thermal front (dashed line).

The vertical distance between the two points where Γ crosses the thermal front is denoted H. Then formula (6) gives:

$$\int_{\Gamma_1} \frac{\mu_1}{k} \bar{q} \cdot d\bar{r} + \int_{\Gamma_o} \frac{\mu_o}{k} \bar{q} \cdot d\bar{r} = (\rho_o - \rho_1)\, gH \qquad (7)$$

Let L_Γ denote the arc length of Γ, and q_Γ a suitable mean tangential component of $\bar{q}$ along Γ. Formula (7) may then be written:

$$q_\Gamma = \frac{k(\rho_o-\rho_1)g}{\mu_o+\mu_1} \cdot \frac{2H}{L_\Gamma} \tag{8}$$

The first factor will appear often in the following. We will call it the characteristic flow q_o:

$$q_o = \frac{k(\rho_o-\rho_1)g}{\mu_o+\mu_1} \tag{9}$$

The buoyancy flow will tilt a thermal front. The rate of tilting is of great interest to us. We need a quantitative measure. This cannot be a very precise concept, since the shape of a front is changing successively. The definition of a tilting rate is necessarily arbitrary to some extent.

Consider a straight thermal front line at a time t. Each point on the front is displaced a length $\bar{v}_T$ dt during a small time increment. The normal displacement is $v_{Tn} \cdot dt$, where v_{Tn} is the thermal velocity component perpendicular to the front line. See Figure 4A and B. Let s, $-\frac{H}{2} \le s \le \frac{H}{2}$, be the coordinate along the straight thermal front. The angular tilting rate, which we are about to define, is denoted ω_t. The front is tilted an angle ω_t dt during the time increment dt. The curved thermal front (Figure 4B) is to be approximated by an appropriate straight line (Figure 4C). The question is how to choose this line. A natural choice is to require that the straight line approximation shall correspond to the same total water flow across the upper and lower halves of the front. Let Q_t denote this tilting flow:

$$Q_t = \int_0^{\frac{H}{2}} q_n(s)\,ds = -\int_{-\frac{H}{2}}^{0} q_n(s)\,ds \tag{10}$$

We assume that the net flow through the front is zero. The formula above should otherwise only include the deviation from an overall mean flow across the thermal front. The equal flow requirement is now:

$$\frac{1}{2}\cdot\frac{H}{2}\cdot\frac{H}{2}\tan(\omega_t dt) = \frac{C_w}{C} Q_t\,dt \tag{11}$$

See Figure 4C.

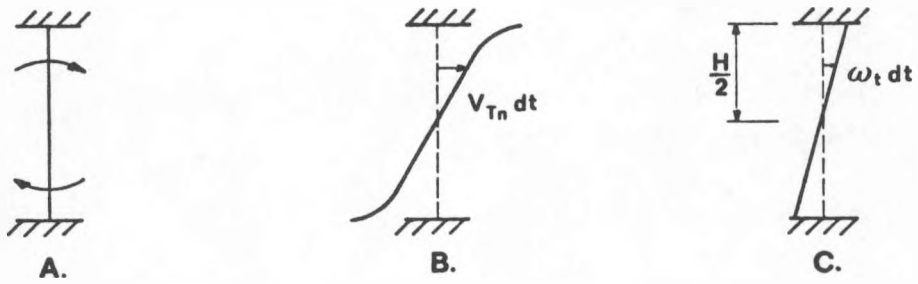

Figure 4. Definition of the angular tilting rate ω_t.
A: Thermal front at a time t.
B: Thermal front at a time t+dt.
C: Linear approximation with the same flow.

The time increment is small so $\tan(\omega_t dt) = \omega_t dt$. We have then the following definition of the tilting rate:

$$\omega_t = \frac{8}{H^2} \cdot \frac{C_w}{C} Q_t \qquad (12)$$

The tilting flow Q_t is the total water flow across the upper half of the straight thermal front. The same amount Q_t passes in the other direction through the lower half of the front.

Let us now briefly discuss the effect of a linear scaling of the aquifer. Let the distances be multiplied by a factor λ. We assume that the temperature field is the same (for corresponding points). Then we get a linear scaling of the pressure, but the flow intensity $\bar{q}$ is unchanged. We have:

$$\begin{array}{ll} L \to \lambda L & P \to \lambda P \\ T \to T & \bar{q} \to \bar{q} \end{array} \qquad \omega_t \to \frac{1}{\lambda}\,\omega_t \qquad (13)$$

We note that the tilting rate is inversely proportional to the linear dimensions.

We will end this section with a brief discussion of the boundary conditions at a sharp thermal front. There are two fundamental requirements. The pressure P must be continuous at the front. The normal component of the water flow must also be continuous. This means that the tangential component of the flow usually is discontinuous at the front. The normal component of the pressure gradient is also discontinuous. We take as an example a vertical sharp thermal front. See Figure 6.

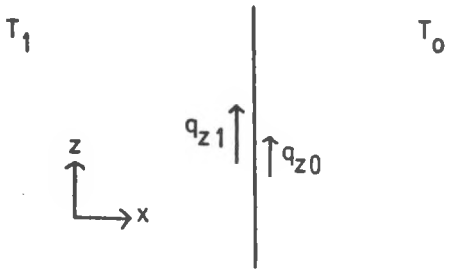

Figure 6. Vertical sharp thermal front.

We have then

$$\frac{k}{\mu_1}\frac{\partial P}{\partial x}\Big|_1 = \frac{k}{\mu_o}\frac{\partial P}{\partial x}\Big|_o \qquad \frac{\mu_1}{k} q_{z1} + \rho_1 g = \frac{\mu_o}{k} q_{z0} + \rho_o g \tag{16}$$

Analytical solutions

It is possible to derive explicit expressions for the pressure distribution and the buoyancy flow pattern in some idealized situations. These solutions are very instructive. They provide a good starting point for the analysis of the thermal stratification problems.

Figure 7 A-F shows the considered cases. There is a warm region with the temperature T_1 and a cold one with the temperature T_o. The density and viscosity are ρ_1, μ_1 and ρ_o, μ_o respectively. The permeability may for all cases except D be different in the horizontal (k) and vertical (k') directions. We will use the notation

$$\kappa = \sqrt{\frac{k'}{k}} \tag{17}$$

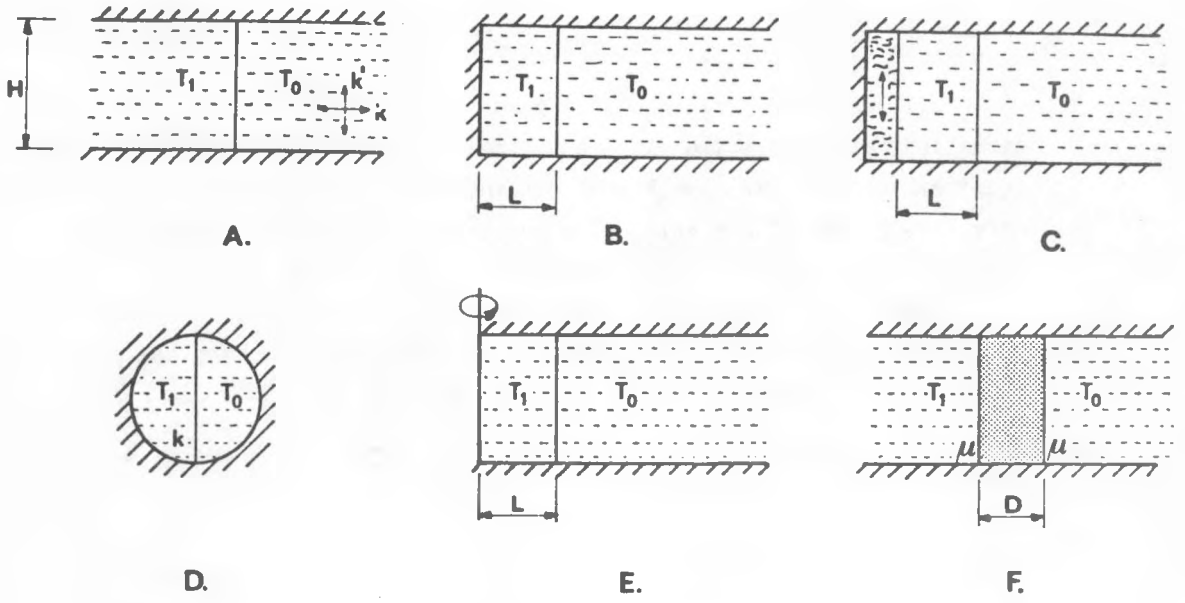

Figure 7, A-F. Considered cases with analytical solutions.

A: Infinite strip.

B: Semi-infinite strip with impermeable left boundary.

C: Semi-infinite strip with free flow in a well along the left boundary.

D: Circular disc.

E: Cylindrical case.

F: Infinite strip with thermal front thickness D.

Case A is an infinite, plane aquifer with a sharp thermal front. The height of the aquifer stratum is H. The expressions for the pressure distribution and the flow field are derived in an appendix. The flow field is shown in figure 8.

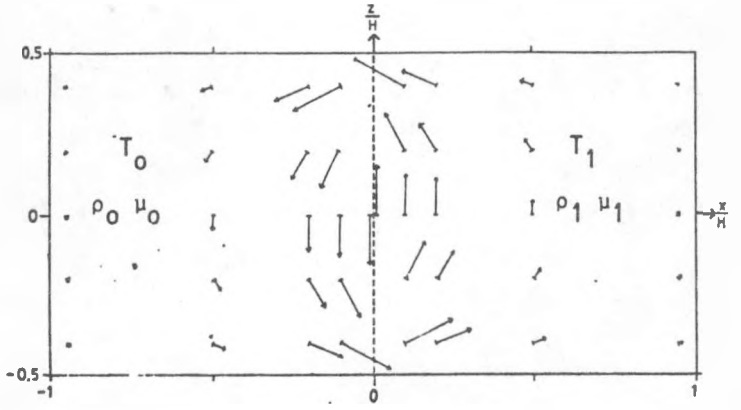

Figure 8. Flow field $\bar{q}/q_0$ in case A (κ=1).

The aquifer region is a plane semi-infinite strip in case B and C. There is a sharp, vertical thermal front. The warmer region to the left has a thickness L. The left boundary is impermeable in case B. There may be a well along the left boundary in which the water flows freely. In this case C the hydrostatic pressure $P = -\rho_1 \cdot gz$ prevails along the left, vertical boundary.

In case D the aquifer is a circular disc. The permeability must in this case be isotropic ($\kappa = 1$).

E is a case with cylindrical symmetry. The warmer region occupies a cylindrical volume with radius L.

In case F we have a plane infinite aquifer. The thermal front has a thickness D. The viscosity must for this case be constant $\mu = \mu_0 = \mu_1$. The density is ρ_1 in the warm region and ρ_0 in the cold one. The density is assumed to increase linearly through the thermal front region.

The analytical solutions for these cases are given in [3]. The given expressions are of course only valid at the considered time with the given thermal front position.

The motion of the thermal front is determined by the intensity of ground water flow across the front. Let z denote the vertical coordinate, and let z = 0 be the mid-point of our thermal fronts. The horizontal ground water flow across the front is denoted $q_f(z)$. This quantity is of first-hand interest to us. We have in the six cases:

A. Infinite strip.

$$q_f(z) = \kappa\, q_0 \cdot \frac{1}{\pi} \ln \left[\frac{1+\sin(\frac{\pi z}{H})}{1-\sin(\frac{\pi z}{H})}\right] \tag{18}$$

B. Semi-infinite strip. Impermeable left boundary.

$$q_f(z) = \kappa\, q_0 \cdot \frac{4}{\pi} \sum_{n=0}^{\infty} \frac{(-)^n}{2n+1} \cdot \frac{\sin\left[\frac{(2n+1)\pi z}{H}\right]}{\frac{\mu_0}{\mu_1+\mu_0} + \frac{\mu_1}{\mu_1+\mu_0} \coth\left[\frac{(2n+1)\pi\kappa L}{H}\right]} \tag{19}$$

C. Semi-infinite strip. Free vertical flow along the left boundary.

$$q_f(z) = \kappa\, q_o \cdot \frac{4}{\pi} \sum_{n=0}^{\infty} \frac{(-)^n}{2n+1} \cdot \frac{\sin\left[\frac{(2n+1)\pi z}{H}\right]}{\frac{\mu_o}{\mu_o+\mu_1} + \frac{\mu_1}{\mu_o+\mu_1} \cdot \tanh\left[\frac{(2n+1)\pi\kappa L}{H}\right]} \qquad (20)$$

D. Circular disc.

$$q_f(z) = q_o \cdot \frac{1}{\pi}\left\{\left[1+\left(\frac{R}{z}\right)^2\right] \cdot \ln\left(\frac{1+\frac{z}{R}}{1-\frac{z}{R}}\right) - 2 \cdot \frac{R}{z}\right\} \qquad (21)$$

E. Cylindrical case.

$$q_f(z) = \kappa\, q_o \cdot \frac{4}{\pi} \sum_{n=0}^{\infty} \frac{(-)^n}{2n+1} \cdot \frac{\sin\left[\frac{(2n+1)\pi z}{H}\right]}{\frac{\mu_1}{\mu_o+\mu_1} \cdot \frac{I_o(\gamma_n)}{I_1(\gamma_n)} + \frac{\mu_o}{\mu_o+\mu_1} \cdot \frac{K_o(\gamma_n)}{K_1(\gamma_n)}} \qquad (22)$$

$$\gamma_n = \frac{(2n+1)\pi\kappa L}{H}$$

Here we have used the modified Bessel functions K_n and I_n.

F. Infinite strip with diffuse thermal front.

$$q_f(z) = \kappa\, q_o \cdot \frac{4}{\pi} \sum_{n=0}^{\infty} \frac{(-)^n}{2n+1} \cdot \frac{1 - e^{-\frac{(2n+1)\pi\kappa\frac{D}{2}}{H}}}{\frac{(2n+1)\pi\kappa\frac{D}{2}}{H}} \cdot \sin\left[\frac{(2n+1)\pi z}{H}\right] \qquad (23)$$

The flow $q_f(z)$ refers to the middle of the thermal front region. For large $\frac{\kappa D}{H}$ we have as a good approximation:

$$q_f(z) \approx 2q_o \cdot \frac{z}{D} \qquad (23')$$

The flows $q_f(z)$ are all odd functions of z. Figures 9-14 show the thermal front flow $q_f(z)$, $0 \le z \le \frac{H}{2}$, in different cases. The curves show the dimensionless flow $q_f/(\kappa q_o)$. The quotient of the viscosities $\beta = \mu_o/\mu_1$ is an important parameter. We will use two values which correspond to the following temperatures:

$$\begin{matrix} T_1 = 90^oC \\ T_o = 5^oC \end{matrix} \quad \beta = \frac{\mu_o}{\mu_1} = 4.82 \qquad \begin{matrix} T_1 = 90^oC \\ T_o = 40^oC \end{matrix} \quad \beta = 2.09 \qquad (24)$$

Values for $\beta = 1$ will also be given for comparison.

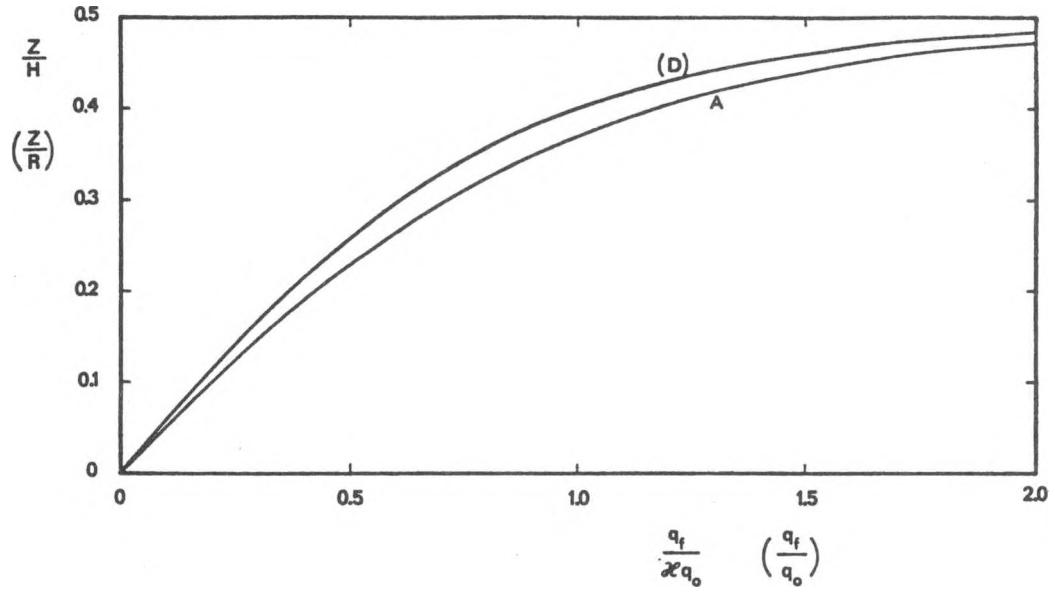

Figure 9. A: Infinite strip.
D: Circular disc.

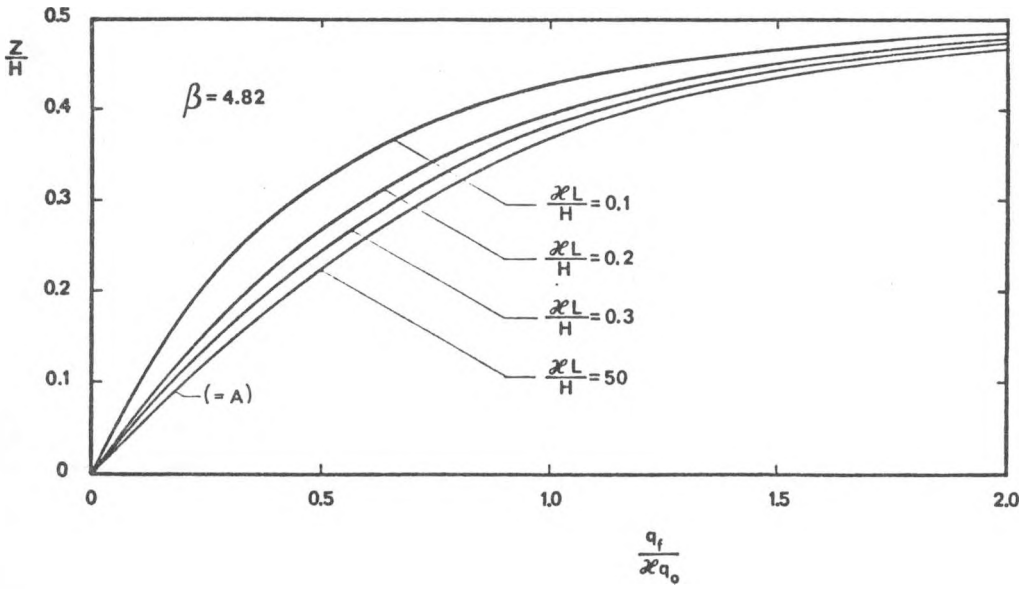

Figure 10. B: Semi-infinite strip with impermeable left boundary.

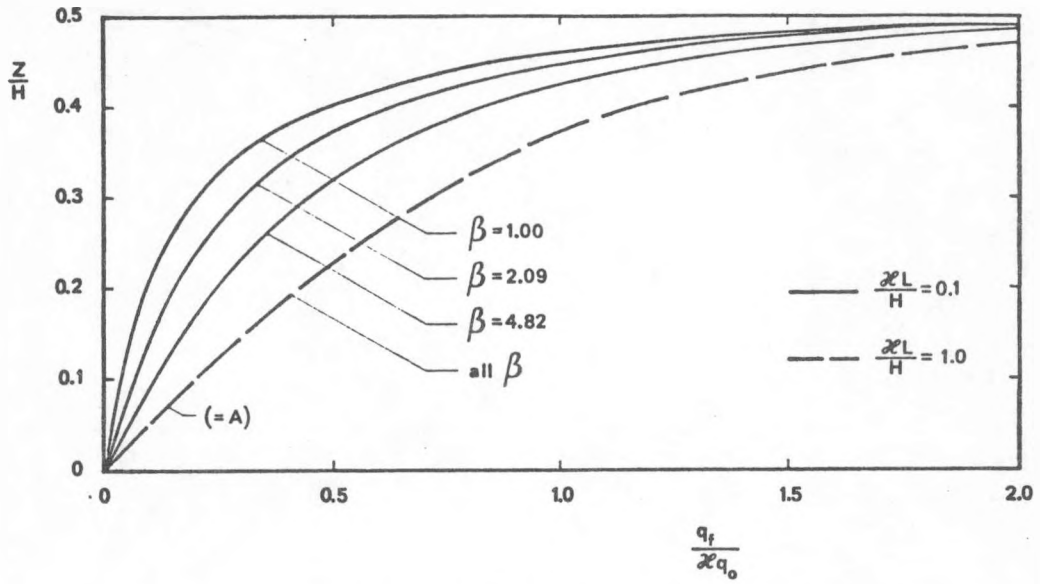

Figure 10'. B: Semi-infinite strip with impermeable left boundary.

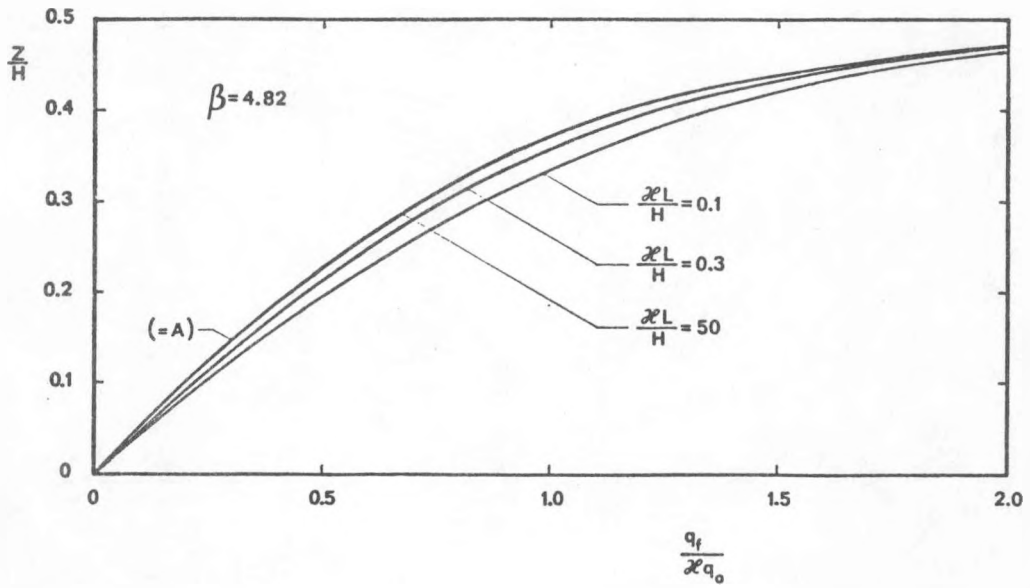

Figure 11. C: Semi-infinite strip with hydrostatic pressure along the left boundary.

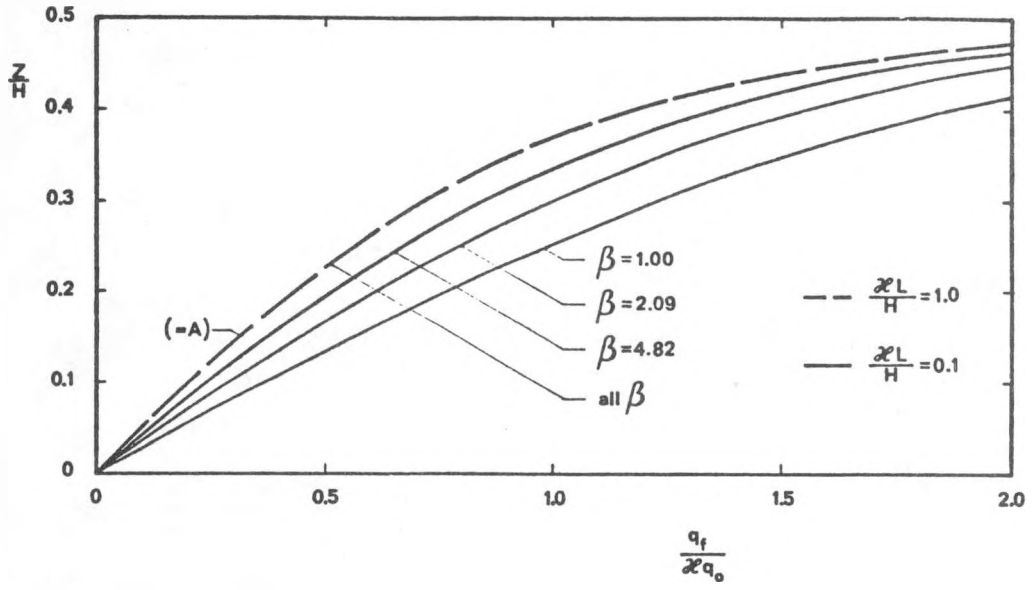

Figure 11': C: Semi-infinite strip with hydrostatic pressure along the left boundary.

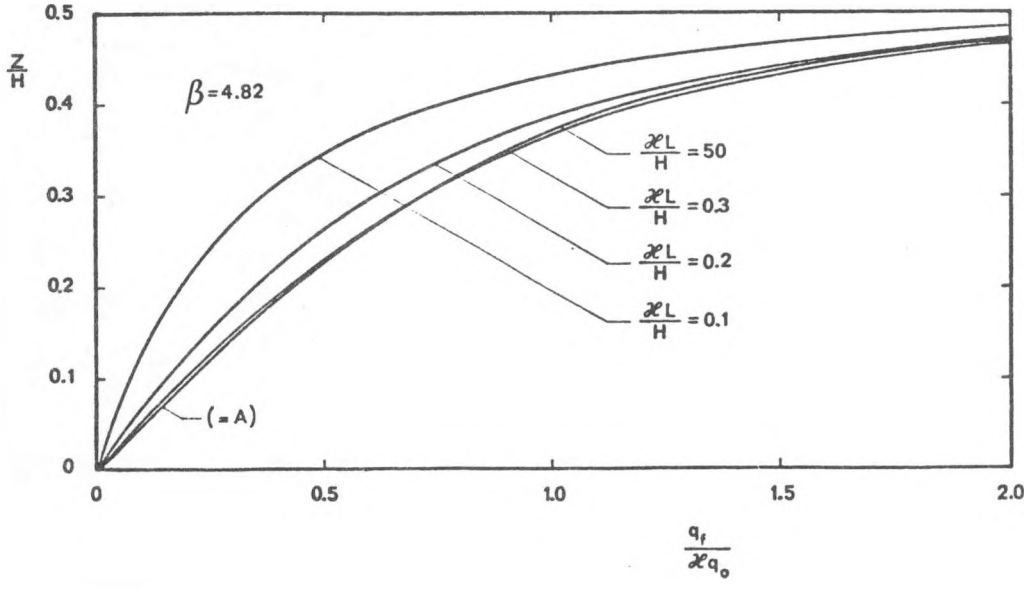

Figure 12: E: Cylindrical case.

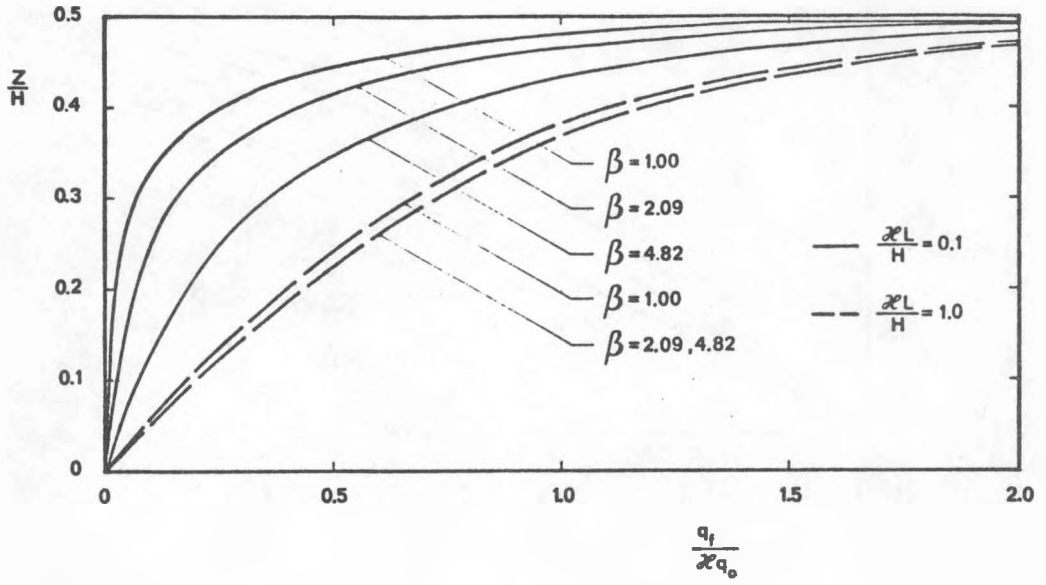

Figure 13: E: Cylindrical case.

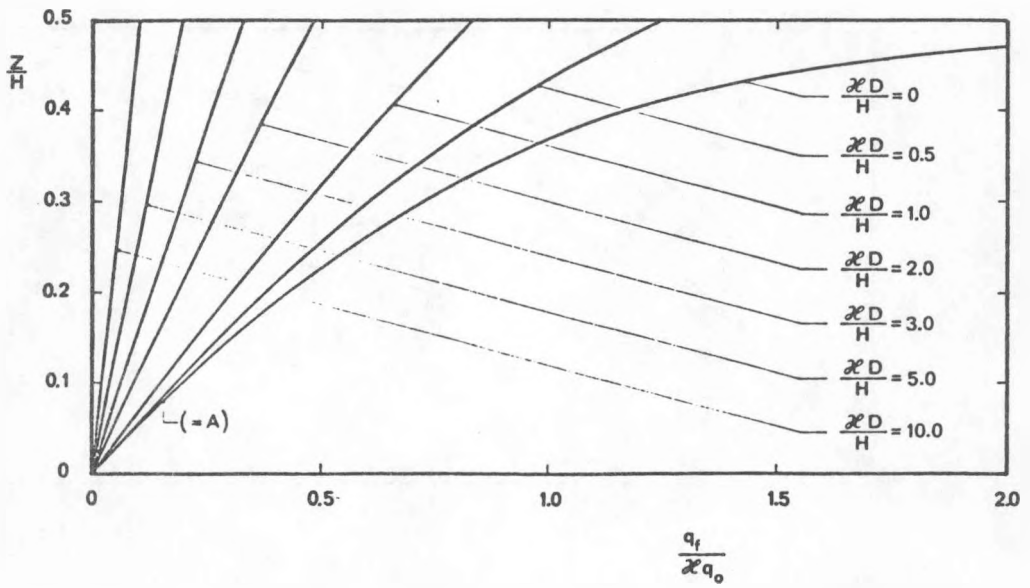

Figure 14. F: Infinite strip with thermal front thickness D.

Figure 9 shows the tilting flow across the thermal front for the infinite strip. This curve is also indicated in the other figures for comparison. The tilting flow is diminished somewhat when the aquifer region is limited to the circular disc of case D. See Figure 9 . The left region with the temperature T_1 has a width L in case B and C. The tilting flow does not differ much from the infinite case A, when $\frac{\kappa L}{H}$ is greater than say 0.3. See Figures 10 and 11. The tilting flow of the cylindrical case E has the same character as the plane case B. See Figures 12, 13. It is clear from Figures 9-13 that the infinite strip case A is a good approximation for the tilting flow except for thin warm regions.

Figure 14 shows the tilting flow for a vertical thermal front with a thickness D. The deviation from the sharp front case A is again rather small, when $\kappa D/H$ is less than say 0.3. The flow increases linearly with z for large $\kappa D/H$ in accordance with formula (23').

We are particularly interested in the rate of tilting ω_t as defined by (12). We need the tilting flow Q_t defined by (10). We have to integrate the flow $q_f(z)$ over the interval $0 \leq z \leq \frac{H}{2}$. The integration of each term in the different series is simple.

We get in case A:

$$Q_t = \frac{4G}{\pi^2} \kappa q_o H \qquad (G = 0.915... \text{ Catalan's constant}) \tag{25}$$

The corresponding rate of angular tilting is:

$$\omega_o = \frac{32G}{\pi^2} \cdot \kappa v_o \cdot \frac{1}{H} \qquad v_o = \frac{C_w q_o}{C} \tag{26}$$

$$(\frac{32G}{\pi^2} \cong 3.0)$$

We will use this tilting rate ω_o as reference in the other cases. The corresponding tilting time t_o is:

$$t_o = \frac{1}{\omega_o} = \frac{HC}{\kappa C_w k} \cdot \frac{\pi^2(\mu_o+\mu_1)}{32G(\rho_o-\rho_1)g} \tag{27}$$

The second factor to the right is a function only of the two temperatures T_o and T_1. Let us use the temperatures 40°C and 90°C as reference. The temperature influence on t_o is expressed by the quotient:

$$\eta = \frac{t_o(T_o,T_1)}{t_o(40,90)} = \frac{\mu(T_o)+\mu(T_1)}{\rho(T_o)-\rho(T_1)} \cdot \frac{\rho(40)-\rho(90)}{\mu(40)+\mu(90)} \qquad (28)$$

The function η is shown in figure 15.

The basic tilting time t_o may be written:

$$t_o = \frac{\eta \cdot HC}{\kappa C_w k} \cdot 1.2 \cdot 10^{-6} \qquad (29)$$

The numerical constant is the second factor of (27) taken for the temperatures $T_o = 40^oC$ and $T_1 = 90^oC$.

The tilting flow in case D becomes:

$$Q_t = \frac{2}{\pi} q_o R \qquad \omega_t = \frac{8}{\pi} \cdot v_o \cdot \frac{1}{2R} \qquad (\frac{8}{\pi} \cong 2.5)$$

The tilting rate is thus reduced in the proportion 2.5/3.0, when we go from the infinite strip (with $\kappa = 1$) to the corresponding circular disc.

The tilting rate ω_t/ω_o is shown in figures 16, 17 and 18 for $\beta = 4.82$, 2.09 and 1.0 respectively for different situations. We note again that the deviation from the tilting rate ω_o of the infinite strip is small, when $\frac{\kappa L}{H}$ is greater than say 0.5.

$\eta = \frac{t_o(T_1,T_o)}{t_o(90,40)}$

T_o(°C)	5	10	20	40	60	90	120	150	170	200
200	-									-
170									-	0.233
150								-	0.457	0.157
120							-	0.422	0.226	0.122
90						-	0.671	0.277	0.186	0.118
60					-	1.22	0.481	0.267	0.197	0.135
40				-	3.39	1	0.500	0.304	0.233	0.166
20			-	7.14	2.62	1.10	0.617	0.398	0.313	0.228
10		-	- 33.3	6.49	2.80	1.28	0.741	0.488	0.385	0.284
5	-	81.3	24.2	6.45	2.96	1.40	0.826	0.546	0.435	0.322

T_1 (°C)

Figure 15. Tilting time function $\eta(T_1, T_o)$. See (27) and (28).

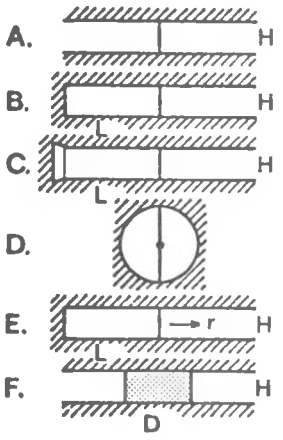

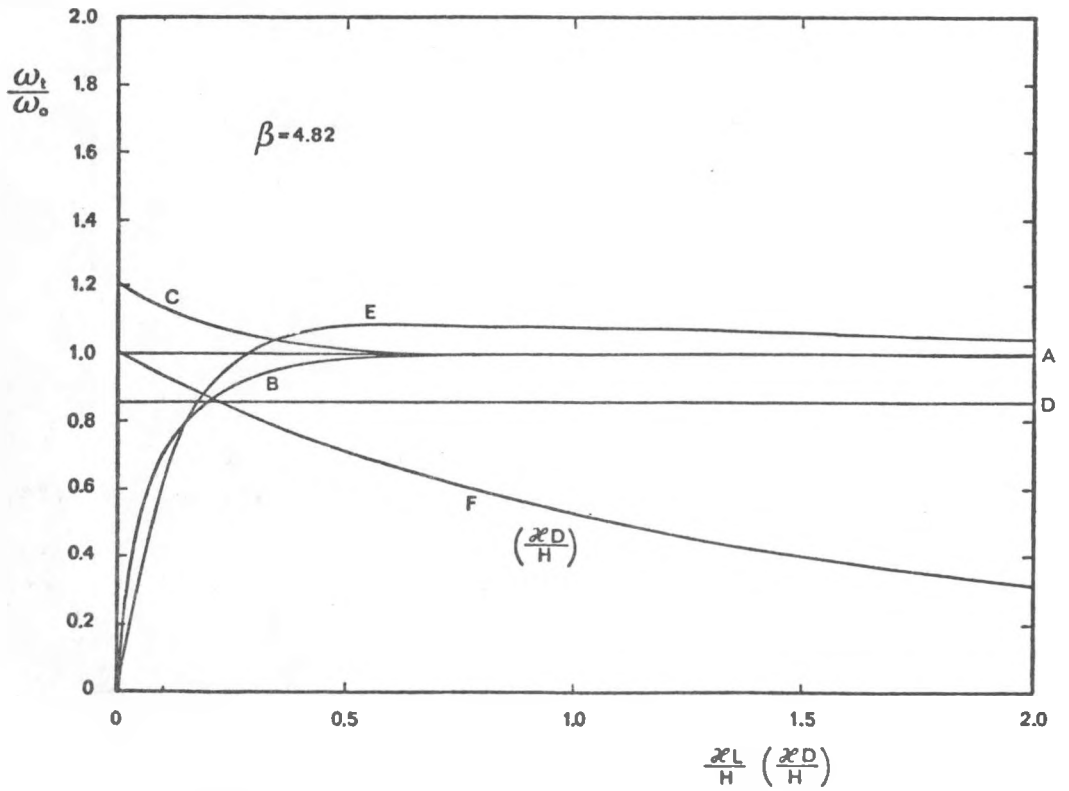

Figure 16. Tilting rate for β=4.82 (T_1=90°C, T_o=5°C)

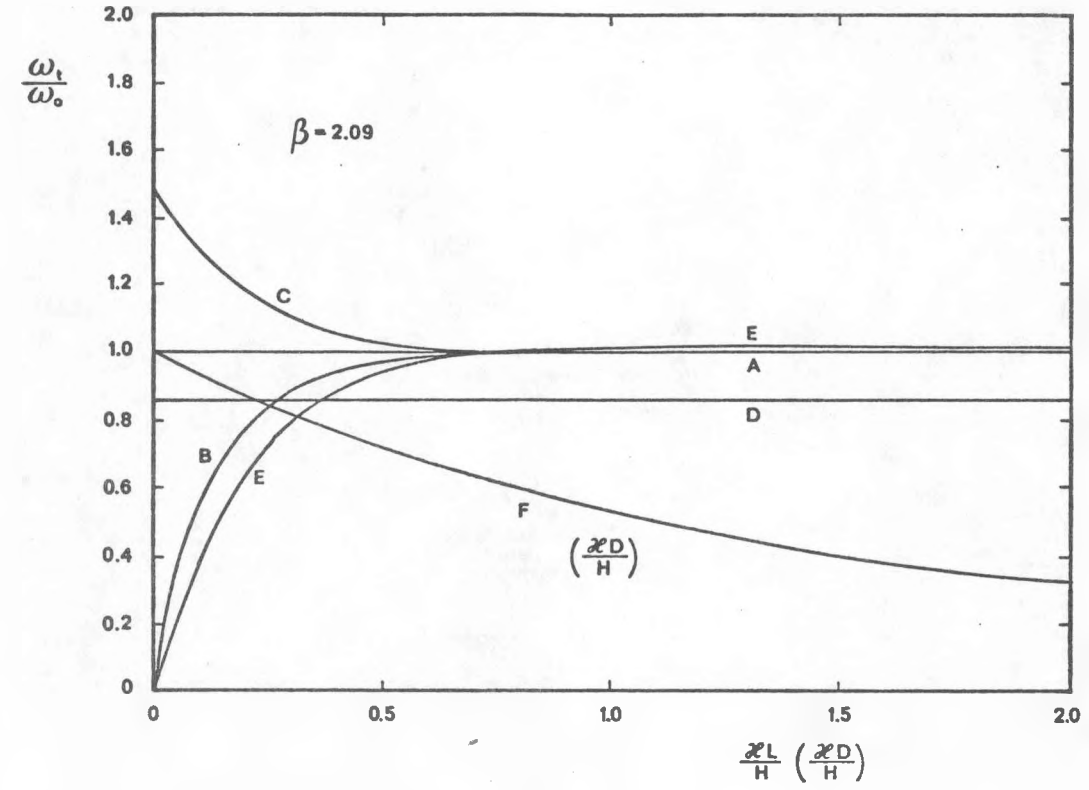

Figure 17. Tilting rate for β=2.09 (T_t=90°C, T_o=40°C).

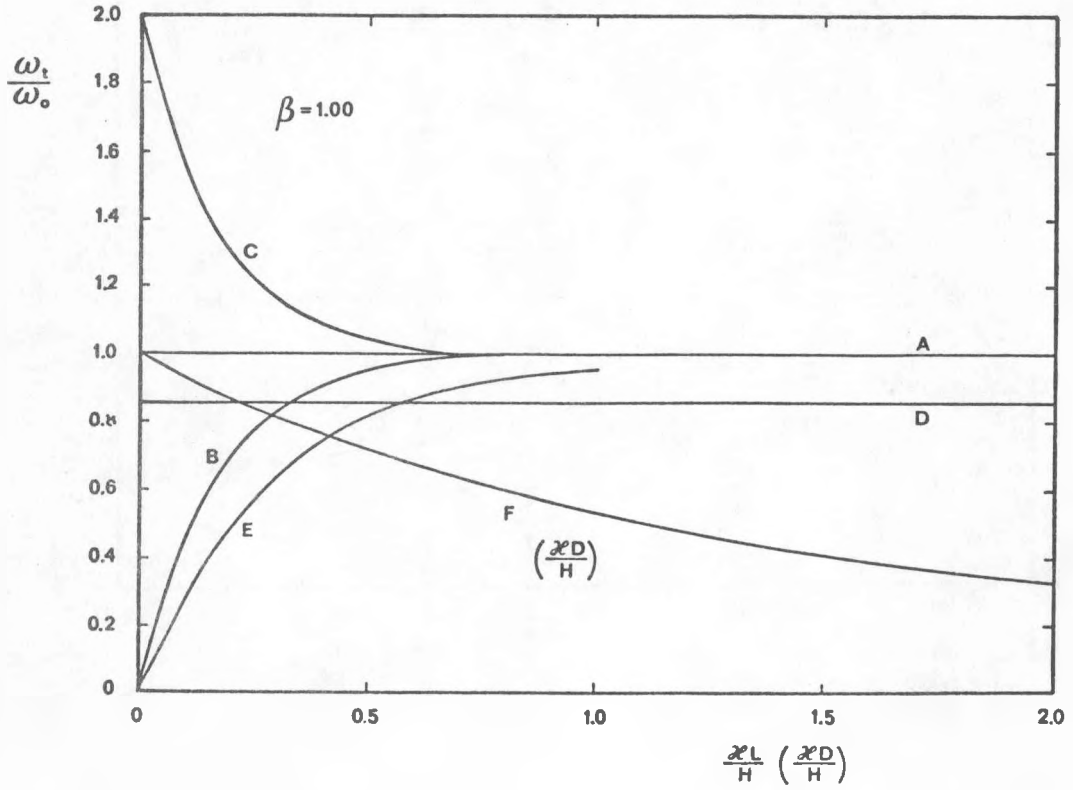

Figure 18: Tilting rate for β=1.

Buoyancy tilting criterion

We are now able to present a buoyancy tilting criterion or, to be more precise, a requirement in order to avoid substantial buoyancy tilting. It should be emphazised that the criterion is not too precise. It should be regarded as an order of magnitude guideline.

Let t_y denote the time period of the storage cycle. For annual storage t_y equals one year: $t_y = 31.5 \cdot 10^6$ s. A reasonable condition is that the basic tilting time t_o shall exceed t_y. A condition in order to avoid substantial buoyancy tilting is then

$$t_o > t_y \tag{30}$$

From (29) we get the condition:

$$\frac{\kappa \, C_w \, k}{\eta \, C \, H} < 0.04 \cdot 10^{-12} \tag{31}$$

The permeability k shall be in m^2 and H in m.

The factor κ depends on the ratio of the vertical and horizontal permeabilities in the aquifer according to formula (17). The heat capacity quotient C_w/C is dimensionless. The factor η contains the dependence on the two temperatures T_o and T_1. See Figure 15. The condition (31) imposes a rather severe limitation on the quotient k/H. Let us in particular put:

$$\eta = 1, \quad \kappa = 1, \quad \frac{C_w}{C} = 1.6 \tag{32}$$

Then we get as a rule of thumb:

$$\frac{k}{H} < \frac{1}{40} \cdot 10^{-12} \tag{33}$$

An aquifer with a permeability of 1 darcy ($k \cong 1.0 \cdot 10^{-12}$ m^2) and a height H = 40 m (and the temperatures $T_o = 40^o$ and $T_1 = 90^o$ C) lies at the limit of the criterion.

Formula (31) is a condition for the permeability. We shall give an alternative expression which instead contains a gradient of the driving hydraulic head. Let h (m/m) denote an appropriate mean gradient of the

driving hydraulic head during injection and extraction periods. We also introduce a corresponding thermal displacement length L_y:

$$L_y = \frac{k}{(\mu_o+\mu_1)/2} \cdot \rho_o g h \cdot \frac{C_w}{C} t_y \qquad (34)$$

The factor $(\mu_o+\mu_1)/2$ is a mean viscosity in the aquifer during a cycle. The quantity L_y/t_y is the thermal velocity, when there is a driving pressure gradient $\rho_o gh$. The length L_y gives the displacement of the thermal front for a pumping during the whole period t_y.

Condition (30) becomes with (34) and (27):

$$\frac{\pi^2}{16\ G} \cong 0.7 > \kappa \cdot \frac{\rho_o-\rho_1}{\rho_o} \cdot \frac{L_y}{hH} \qquad (35)$$

The criteria (30)-(35) are based on the tilting rate of a sharp, vertical front. Only pure buoyancy is influencing the tilting rate. We will in the following sections discuss the more complicated situation with a sloping thermal front for which both buoyancy and forced convection influence the tilting.

Superposition of buoyancy and forced convection

The ground water flow in the aquifer is a combination of forced and natural convection during periods of injection and extraction. One may at each time regard the flow as a combination of a pure buoyancy flow and a forced convection.

The pure buoyancy flow has been discussed in detail. It is of the same character during injection/extraction and storage periods. It is at work all the time and strives to tilt the thermal front so that the warm water ends on top.

The pure buoyancy part takes care of the density variations in the aquifer. The other part, the forced convection, is not influenced by the density variations. Let P_b and P_{fc} be the two contributions to the total pressure:

$$P = P_b + P_{fc} \qquad (36)$$

The two components satisfy the equations:

$$\nabla \cdot \left[\frac{k}{\mu}(\nabla P_b + \rho g \hat{z})\right] = 0 \qquad (37)$$

$$\nabla \cdot \left[\frac{k}{\mu} \nabla P_{fc}\right] = 0 \qquad (38)$$

The equations (37) and (38) are for simplicity written for the isotropic case. In the case with vertical anisotropy we have to use k' for the z-component in accordance with (2).

The two equations (37) and (38) of the superposition (36) have different characters. Equation (38) for P_{fc} is linear. The pressure P_{fc} and the corresponding forced-convection flow are proportional to the magnitude of the injected and extracted water at the boundary wells. Equation (37) for P_b has a source term from the variable density. The pressure P_b and the corresponding buoyancy flow is proportional to the driving density difference $\rho_0-\rho_1$ between the cold and warm regions.

We are particularly interested in the case of Figure 19. The aquifer occupies an infinite, plane strip. The sharp thermal front is tilted an angle α. A volume Q_1 ($m^3/s,m$) of water is pumped through the strip from left to right.

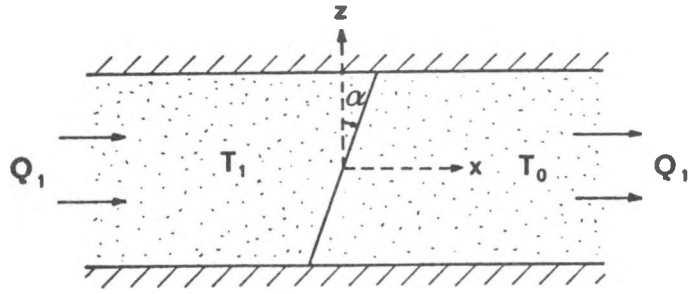

Figure 19. Aquifer strip with tilted thermal front. The volume Q_1 of water is pumped through the strip.

The volumetric ground water flow $\bar{q}$ has two components:

$$\bar{q} = \bar{q}_b + \bar{q}_{fc} \qquad (39)$$

The forced-convection part $\bar{q}_{fc}$ is the solution of (38). The flow is constant and horizontal ($\bar{q}_{fc} \to Q_1/H \cdot \hat{x}$) in the undisturbed regions far away from the front to the right and to the left. The buoyancy part $\bar{q}_b$ is the solution of (37). It becomes zero far away from the front.

A dimensional analysis will be of great use in the following. The dimensionless coordinates are x/H and z/H. The tilting angle α, the viscosity ratio $\beta=\mu_o/\mu_1$, and the permeability quotient $\kappa=\sqrt{k/k}$ are independent parameters. We may write:

$$\bar{q}_b = q_o \cdot \bar{q}'(\frac{x}{H}, \frac{z}{H}, \alpha, \beta, \kappa) \tag{40}$$

$$\bar{q}_{fc} = \frac{Q_1}{H} \bar{q}'' (\frac{x}{H}, \frac{z}{H}, \alpha, \beta, \kappa) \tag{41}$$

The characteristic buoyancy flow q_o is defined by (9). The flows $\bar{q}'$ and $\bar{q}''$ are dimensionless. It is not difficult but rather lengthy to show that they only depend on the five given parameters.

We need a definition of the tilting rate for the sloping thermal front of Figure 19. Consider a vertical cut through the mid-point of the thermal front. Let Q_+ and Q_- denote the flow rate over the upper and lower halves of the vertical cut. We have:

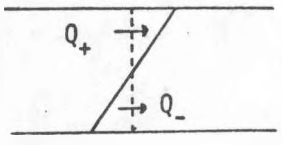

$$Q_+ = \frac{Q_+ + Q_-}{2} + \frac{Q_+ - Q_-}{2}$$

$$Q_- = \frac{Q_+ + Q_-}{2} - \frac{Q_+ - Q_-}{2}$$

The tilting flow is then:

$$Q_t = \frac{Q_+ - Q_-}{2} \tag{42}$$

Let $d\alpha$ be the change of tilting angle during a time increment dt. Consider the two triangles between the thermal front and the vertical cut. The area of these congruent triangles increases, when the tilting angle changes from α to $\alpha+d\alpha$. Heat balance gives:

$$\frac{1}{2} \cdot \frac{H}{2} \cdot \frac{H}{2} (\tan(\alpha+d\alpha) - \tan(\alpha)) \cdot C(T_1 - T_o) = C_w (T_1 - T_o) Q_t dt$$

or

$$\frac{d}{dt} (\tan\alpha) = \frac{8C_w}{H^2 C} \cdot Q_t \tag{43}$$

The tilting flow Q_t has in general a component Q_{bt} from the buoyancy flow and a component Q_{ft} from the forced convection:

$$Q_t = Q_{bt} + Q_{ft} \tag{44}$$

The two components are obtained from (40) and (41). We shall integrate over the upper (or lower) part $0 \leq z \leq H/2$ for x=0. We get immediately:

$$Q_{bt} = q_o H \cdot f_{bt}(\alpha, \beta, \kappa) \tag{45}$$

$$Q_{ft} = Q_1 \cdot f_{ft}(\alpha, \beta, \kappa) \tag{46}$$

The two functions f_{bt} and f_{ft} depend only of the dimensionless parameters α, β, and κ.

The forced tilting is zero for a vertical front $\alpha=0$. We have from (25):

$$f_{bt}(0, \beta, \kappa) = \frac{4G}{\pi^2} \kappa \tag{47}$$

$$f_{ft}(0, \beta, \kappa) = 0$$

The variation of tilting angle with time is determined by (43) to (46) for the present case of a sharp front in an infinite aquifer strip. We need to know the two functions $f_{bt}(\alpha, \beta, \kappa)$ and $f_{ft}(\alpha, \beta, \kappa)$. We will in the following section show that they are related to each other by a simple formula.

Stable front solution

Consider again our plane, infinite strip with a sloping thermal front as shown in Figure 19.

Let us investigate, if it is possible to have a constant, horizontal flow along the aquifer. We assume

$$\bar{q} = \frac{Q_1}{H} \hat{x} \tag{48}$$

This simple flow is assumed to prevail throughout the aquifer strip.

We use the coordinates (x, z) of Figure 19. The pressure in the warm region must satisfy:

$$q_x = \frac{Q_1}{H} = -\frac{k}{\mu_1} \frac{\partial P}{\partial x} \tag{49}$$

$$q_z = 0 = -\frac{k'}{\mu_1} \left(\frac{\partial P}{\partial z} + \rho_1 g\right) \tag{50}$$

See (2). The pressure is then, except for an integration constant:

$$P = -\rho_1 gz - \frac{\mu_1 Q_1}{kH} x \tag{51}$$

In the cold region to the right we have in the same way:

$$P = -\rho_0 gz - \frac{\mu_0 Q_1}{kH} x \tag{52}$$

The thermal front is given by $x=\tan(\alpha)\cdot z$, $-H/2 \leq z \leq H/2$. The normal component of the flow and the pressure must be continuous at the front. The flow is constant. The remaining requirement of continuous pressure at the front gives with (51) and (52):

$$-\rho_1 gz - \frac{\mu_1 Q_1}{kH}\cdot\tan(\alpha)z = -\rho_0 gz - \frac{\mu_0 Q_1}{kH} \tan(\alpha)\, z \tag{53}$$

or with (9):

$$\tan(\alpha) = -\frac{q_0 H}{Q_1} \cdot \frac{\beta+1}{\beta-1} \tag{54}$$

We have, when (54) is satisfied, the simple horizontal flow (48).

The tilting angle of formula (54) is negative, when the forced flow Q_1 is positive. Figure 20 illustrates the physical situation. The buoyancy flow rotates the front clockwise ($\rho_1<\rho_0$). The forced convection displaces the front downstream. The viscosity is smaller to the left ($\mu_1<\mu_0$). The flow in the lower protruding warm edge is enhanced. More water passes the lower half than the upper one. This gives a counter-clockwise rotation of the front. The buoyancy and forced-convection effects oppose each other, when the tilting angle is negative. The two effects balance, when the angle α satisfies (54).

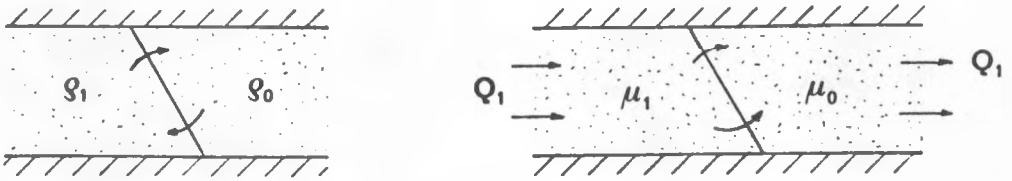

Figure 20. Clockwise rotation due to buoyancy flow (left, $\rho_1<\rho_0$). Counter-clockwise rotation due to forced convection (right, $\mu_1<\mu_0$).

Formula (54) may be used to deduce a relation between the two tilting functions f_{bt} and f_{ft} of formulas (45) and (46). Consider a certain case when, except for Q_1, all variables α, β, κ, q_o and so on are given. Let us choose the pumping rate Q_1 so that (54) is satisfied. The flow is then given by (48). The thermal front will be displaced downstream, but it will not be rotated. The tilting flow Q_t is zero. We have with (45) and (46):

$$Q_t = q_o H \cdot f_{bt}(\alpha, \beta, \kappa) + (-) \frac{q_o H}{\tan(\alpha)} \cdot \frac{\beta+1}{\beta-1} f_{ft}(\alpha, \beta, \kappa) = 0 \qquad (55)$$

The value of Q_1 from (54) has been inserted.

From (55) we get the remarkable formula:

$$f_{bt}(\alpha, \beta, \kappa) = \frac{1}{\tan(\alpha)} \cdot \frac{\beta+1}{\beta-1} \cdot f_{ft}(\alpha, \beta, \kappa) \qquad (56)$$

The formula is of course valid for any values of α, β, and κ.

The function $f_{ft}(\alpha, \beta, \kappa)$ will be computed numerically below. The buoyancy flow function f_{bt} is obtained from (56). We will in the next paragraph analyse the effect of vertical anisotropy before the function f_{ft} is computed numerically.

Effect of vertical anisotropy

The permeability k' in the vertical direction may differ from the permeability k in the horizontal directions. See formula 2. It is however possible to transform an anisotropic case to an isotropic one.

We start with a case with the permeabilities k and k'. The quotient $\kappa = \sqrt{k'/k}$ differs from 1. In aquifer applications one often has $\kappa<1$. We have the coordinates x, y, and z, the pressure distribution P and the flow $\bar{q} = (q_x, q_y, q_z)$.

The horizontal coordinates are contracted with the factor κ. The new system has the coordinates:

$$x' = \kappa x \quad . \quad y' = \kappa y \qquad z' = z \qquad (57)$$

Let us consider the following ground water flow problem in the new coordinates. The pressure in corresponding points are unchanged. The flow in the horizontal plane is increased by the factor $1/\kappa$, while the vertical flow is increased $1/\kappa^2$:

$$P'(x', y', z') = P(x, y, z)$$
$$q_x' = \frac{1}{\kappa} q_x \qquad q_y' = \frac{1}{\kappa} q_y \qquad q_z' = \frac{1}{\kappa^2} q_z \tag{58}$$

The new flow $\bar{q}'$ satisfies the mass conservation equations (3), since:

$$\frac{\partial q_x'}{\partial x'} + \frac{\partial q_y'}{\partial y'} + \frac{\partial q_z'}{\partial z'} = \frac{1}{\kappa} \frac{\partial}{\partial x} \left(\frac{1}{\kappa} q_x\right) + \frac{1}{\kappa} \frac{\partial}{\partial y} \left(\frac{1}{\kappa} q_y\right) + \frac{\partial}{\partial z} \left(\frac{1}{\kappa^2} q_z\right)$$
$$= \frac{1}{\kappa^2} \nabla \cdot \bar{q} = 0 \tag{59}$$

The Darcy relations for $\bar{q}'$ become from (58) and (2):

$$q_x' = \frac{1}{\kappa} \cdot \frac{-k}{\mu} \cdot \frac{\partial P}{\partial x} = - \frac{k}{\mu} \cdot \frac{\partial P'}{\partial x'}$$
$$q_y' = \frac{1}{\kappa} \cdot \frac{-k}{\mu} \cdot \frac{\partial P}{\partial y} = - \frac{k}{\mu} \cdot \frac{\partial P'}{\partial y'} \tag{60}$$
$$q_z' = \frac{1}{\kappa^2} \cdot \frac{-k'}{\mu} \left(\frac{\partial P}{\partial z} + \rho g\right) = - \frac{k}{\mu} \left(\frac{\partial P'}{\partial z'} + \rho g\right)$$

The new ground water flow problem has the isotropic permeability k.

We have the following result. Consider a certain ground water flow problem with a vertical anisotropy. Let the horizontal lengths be contracted by the factor κ. The pressure distribution is unchanged. The horizontal flows are increased $1/\kappa$ and vertical flow $1/\kappa^2$. Then the new flow problem has the isotropic permeability k. When applying this in a certain case one has to pay particular attention to the boundary conditions.

The result may also be expressed in the following way. Suppose we know the flow pattern for a certain isotropic problem with horizontal lengths κL_1, κL_2 and so on. Let q_x, q_y, and q_z be the flow components. Then there is a solution to the corresponding anisotropic case ($\kappa = \sqrt{k/k}$) with the extended horizontal lengths L_1, L_2 and so on, which has the flow components κq_x, κq_y, and $\kappa^2 q_z$.

We will apply this for our case with a sharp thermal front in a plane, infinite aquifer with vertical anisotropy. The front is tilted an angle α. We can transform the problem to an isotropic one by a horizontal contraction κ. This means that the tilting angle changes to a new value α' according to

$$\tan(\alpha') = \kappa \tan(\alpha) \tag{61}$$

Let us first treat the buoyancy tilting ($Q_1=0$). The tilting flow of the original problem is from (45):

$$Q_{bt} = q_o H \cdot f_{bt}(\alpha, \beta, \kappa) \tag{62}$$

The boundary conditions are that the normal flow is zero at $z=\pm H/2$ and that the flow vanishes far away from the front. The boundary conditions are directly fulfilled in the transformed problem. The tilting flow is

$$Q'_{bt} = q_o H \cdot f_{bt}(\alpha', \beta, 1) \tag{63}$$

But we also have that the horizontal flow is enhanced by $1/\kappa$:

$$Q'_{bt} = \frac{1}{\kappa} Q_{bt} \tag{64}$$

From (62)-(64) we have the important relation:

$$f_{bt}(\alpha, \beta, \kappa) = \kappa\, f_{bt}(\alpha', \beta, 1) \tag{65}$$

This relation gives the effect of anisotropy on the buoyancy flow. From (56), (61), and (65) we have for the forced convection:

$$f_{ft}(\alpha, \beta, \kappa) = f_{ft}(\alpha', \beta, 1) \tag{66}$$

The κ-factor of (65) does not appear in this case. Formula (66) could also have been derived directly in the same way as (65). One must then remember the boundary condition with given pumping rate Q_1.

The two functions $f_{ft}(\alpha, \beta, \kappa)$ and $f_{bt}(\alpha, \beta, \kappa)$ are now reduced to one unknown function $f_{ft}(\alpha, \beta, 1)$. The two remaining independent variables are the tilting angle α and the viscosity ratio β. The following section is devoted to a study of $f_{ft}(\alpha, \beta, 1)$.

Forced-convection tilting

The partial differential equation for the pressure P_{fc} for the forced-convection component is given by (38). We consider only the isotropic case $\kappa=1$. Figure 19 shows the plane, infinite aquifer strip with a sharp, sloping thermal front. There is a constant horizontal flow Q_1/H in the undisturbed aquifer far away from the thermal front. The vertical component of the flow is zero at the horizontal boundaries $z=\pm H/2$.

The pressure distribution P_{fc} and the flow pattern have been computed numerically with the use of forward differences. A mesh with about 3000 points has been used. Figure 21 shows the type of flow pattern that we get.

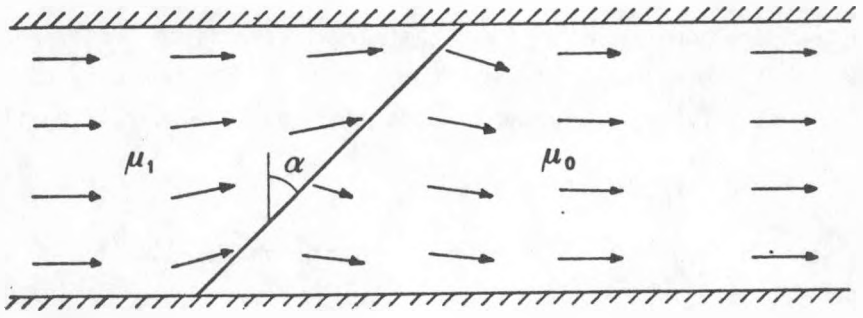

Figure 21. Ground water flow pattern for forced convection in an aquifer strip with a sloping thermal front.

The tilting angle of the thermal front is α. The viscosity is lower in the warm region to the left ($\mu_1 < \mu_0$). The flow resistance is smaller in the warm upper part around the thermal front. The flow becomes stronger in the upper half, and we get a tilting flow as shown in Figure 21.

The tilting flow Q_{ft} is defined by (42). The forced-convection tilting function is from (46):

$$f_{ft}(\alpha, \beta, 1) = Q_{ft}/Q_1 \tag{67}$$

Here Q_1 ($m^3/m,s$) denotes the total volume of water that is pumped along the aquifer.

The numerical calculations have been made for two viscosity ratios. The value $\beta=2.09$ is obtained for $T_1=90^oC$ and $T_0=40^oC$, while $\beta=4.82$ is obtained for $T_1=90^oC$ and $T_0=5^oC$. The calculations were made for several angles α. Table I shows the result.

$\beta=\frac{\mu_0}{\mu_1}$	α 0^o	15^o	30^o	45^o	60^o	75^o	90^o
2.09	0	.033	.067	.099	.131	.158	.176
4.82	0	.061	.125	.189	.251	.302	.328

Table I. The function $f_{ft}(\alpha, \beta, 1)$ which gives the tilting flow as a function of the tilting angle α and the viscosity ratio β. Isotropic case ($\kappa=1$).

The function f_{ft} is zero for a vertical front (47). We get the derivative with respect to α, if we take the limit $\alpha \to 0$ in (56). We get with the use of (47):

$$\frac{\partial f_{ft}(0,\beta,1)}{\partial \alpha} = \frac{4G}{\pi^2} \cdot \frac{\beta-1}{\beta+1} \tag{68}$$

The limiting case with a horizontal front ($\alpha=90^o$) is simple. The flows in the upper and lower halves are inversely proportial to the viscosities: $Q_+/Q_- = \mu_o/\mu_1$. From this we get:

$$f_{ft}(90^o, \beta, \kappa) = \frac{1}{2} \cdot \frac{\beta-1}{\beta+1} \tag{69}$$

The tilting rate formulas in the following section will contain the quantity:

$$\frac{\pi^2}{4G} \cdot \frac{1}{\tan(\alpha)} \cdot \frac{\beta+1}{\beta-1} \cdot f_{ft}(\alpha, \beta, 1) \tag{70}$$

In figure 22 we have plotted this expression from the values of table I. We have chosen $s=\tan(\alpha)$ as independent variable.

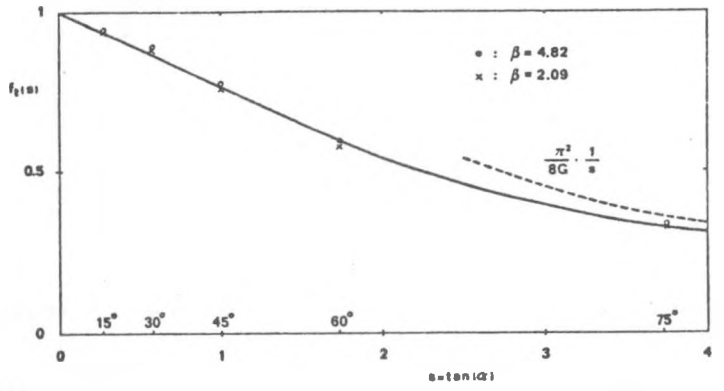

Figure 22. The quantity (70) as a function of $s=\tan(\alpha)$. The full line gives the basic tilting function $f_t(s)$.

We see that the points for the two values of β lie very close to each other. It is reasonable to approximate expression (70) with a single curve. We have with very good accuracy:

$$f_{ft}(\alpha, \beta, 1) = \frac{4G}{\pi^2} \tan(\alpha) \frac{\beta-1}{\beta+1} \cdot f_t(\tan\alpha) \tag{71}$$

We will call $f_t(s)$ the basic tilting function. It is shown in figure 22.

From the basic tilting function we get with formulas (71), (66), (61), and (56) the two tilting functions $f_{ft}(\alpha, \beta, \kappa)$ and $f_{bt}(\alpha, \beta, \kappa)$.

The value $f_t(0)$ is obtained from the derivative of (71) with respect to α at the point $\alpha=0$. We have with (68):

$$f_t(0) = 1 \tag{72}$$

The asymptotic value of $f_t(s)$ for large s is from (69) and (71) of the form $\pi^2/(8Gs)$. The dashed curve in Figure 22 shows this asymptot. We note from the figure that $f_t(s)$ is linear in the interval $0 \leq s \leq 2$. We have with good accuracy:

$$f_t(s) \approx 1 - f_1 \cdot s \qquad 0 \leq s \leq 2 \tag{73}$$

$$f_1 = 0.235$$

The function $f_t(s)$ is given in table II.

α^o	0	15	30	45	60	75	90
$s=\tan\alpha$	0	0.268	0.577	1.000	1.732	3.732	∞
$f_t(s)$	1	0.937	0 864	0.765	0.593	0.329	0

Table II. The basic tilting function $f_t(s)$.

Tilting rate formula

We are now in the position to give a relatively simple formula for the tilting rate of the thermal front. The discussion in the present section concerns the case shown in Figure 19.

We have an infinite aquifer strip with a sharp thermal front. The tilting angle is a function of time: $\alpha=\alpha(t)$. The aquifer may exhibit a vertical anisotropy ($\kappa \neq 1$). The total forced-convection flow along the aquifer is Q_1. The value of Q_1 may be positive, zero, or negative. The combined effect of buoyancy and forced convection is considered.

The effects of the diffuseness of the thermal front, of a vertical left boundary at finite distance from the front, and of cylindrical symmetry instead of the present plane case are not included in the

present considerations. An approximate treatment of these additional complications are given in a following section.

The equation for the change of the tilting angle is given by (43). The tilting flow is obtained from (44)-(46). The two tilting functions $f_{bt}(\alpha, \beta, \kappa)$ and $f_{ft}(\alpha, \beta, \kappa)$ are connected to each other through (56). The anisotropy dependence is given by (66) and (61). Finally we get with the use of (71), the basic tilting function $f_t(s)$, and the basic tilting time t_o (27) the following equation for $\alpha(t)$:

$$\frac{d}{dt}(\tan\alpha) = \frac{1}{t_o} f_t(\kappa\tan\alpha)\cdot\left[1+\frac{Q_1}{q_o H}\cdot\frac{\beta-1}{\beta+1}\tan\alpha\right] \tag{74}$$

Let us use the variable

$$s = \kappa\tan(\alpha) \tag{75}$$

We also introduce the parameter:

$$\gamma = \frac{Q_1}{\kappa q_o H}\cdot\frac{\beta-1}{\beta+1} \tag{76}$$

The quantity γ is a measure of the forced-convection flow Q_1/H compared to the characteristic buoyancy flow q_o. If we insert (9), we have instead:

$$\gamma = \frac{Q_1}{\kappa k g H}\cdot\frac{\mu_o-\mu_1}{\rho_o-\rho_1} \tag{77}$$

Using the characteristic tilting time (27), we have:

$$\gamma = \frac{32G}{\pi^2}\cdot\frac{\beta-1}{\beta+1}\cdot\frac{Q_1 C_w t_o}{H^2 C} \tag{78}$$

The last factor of (78) has the following physical interpretation. The horizontal volumetric flow is Q_1/H. The corresponding thermal velocity is $Q_1 C_w/(HC)$. The thermal front is displaced a distance $Q_1 C_w t_o/(HC)$ during the characteristic tilting time. The last factor of (78) is therefore the quotient of this displacement and the height H of the aquifer strip.

We may write (74) in the follwing way:

$$\frac{ds}{dt} = \frac{\kappa}{t_o}\cdot f_t(s)(1+\gamma s) \tag{79}$$

The basic tilting function $f_t(s)$ is given by Figure 22 and Table II. We note that the tilting $s = \kappa\tan(\alpha)$ is a function of the dimensionless time $\kappa t/t_o$. There is only one parameter γ.

Equation (79) is solved in the following way. Formula (79) may be rewritten:

$$\frac{ds}{f_t(s)(1+\gamma s)} = \frac{\kappa}{t_0}\,dt \tag{80}$$

We introduce the following integral:

$$S(s,\gamma) = \int_0^s \frac{ds'}{f_t(s')(1+\gamma s')} \tag{81}$$

The variable s is positive: $0 \leq s < \infty$. The parameter γ may assume any value: $-\infty < \gamma < \infty$. The integrand becomes, for negative γ, infinite, when $s' = -1/\gamma$. The integral is infinite for $s = -1/\gamma$. We get one curve for $0 \leq s < -1/\gamma$ and another one for $-1/\gamma < s < \infty$. See Figure 23.

We can use approximation (73), when $0 \leq s \leq 2$. The integration of (81) is then elementary. We have:

$$S(s,\gamma) = \frac{1}{\gamma + f_1} \cdot \ln\left(\frac{|1+\gamma s|}{1-f_1 s}\right) \tag{82}$$

$(f_1 = 0.235) \qquad 0 \leq s \leq 2$

Expression (82) is not defined, when $\gamma = -f_1$. Then we have by direct integration:

$$S(s,-f_1) = \frac{s}{1-f_1 s} \tag{82'}$$

The function $S(s,\gamma)$ is shown in Figure 23.

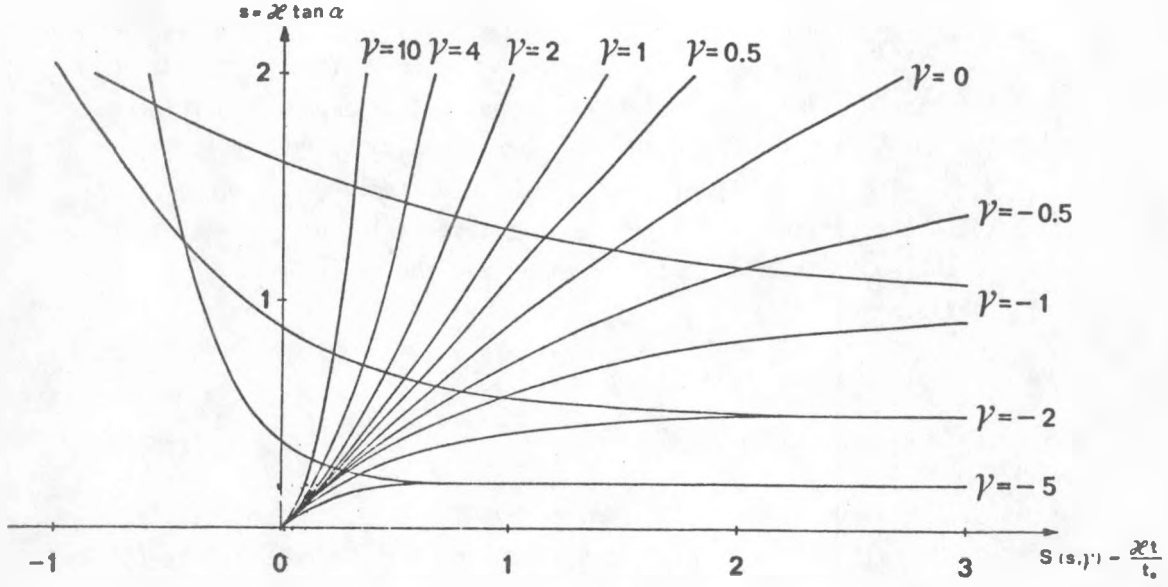

Figure 23. The function $S(s,\gamma)$. See (81) and (82).

The solution of (79) during a period with constant γ is with (80) and (81) given by:

$$S(s_2,\gamma) - S(s_1,\gamma) = \frac{\kappa(t_2-t_1)}{t_o} \qquad (83)$$

$$s_2 = s(t_2) \qquad s_1 = s(t_1)$$

The tilting $s = \kappa\tan\alpha$ will follow the curves of Figure 23. Figure 24 illustrates what happens during a storage cycle.

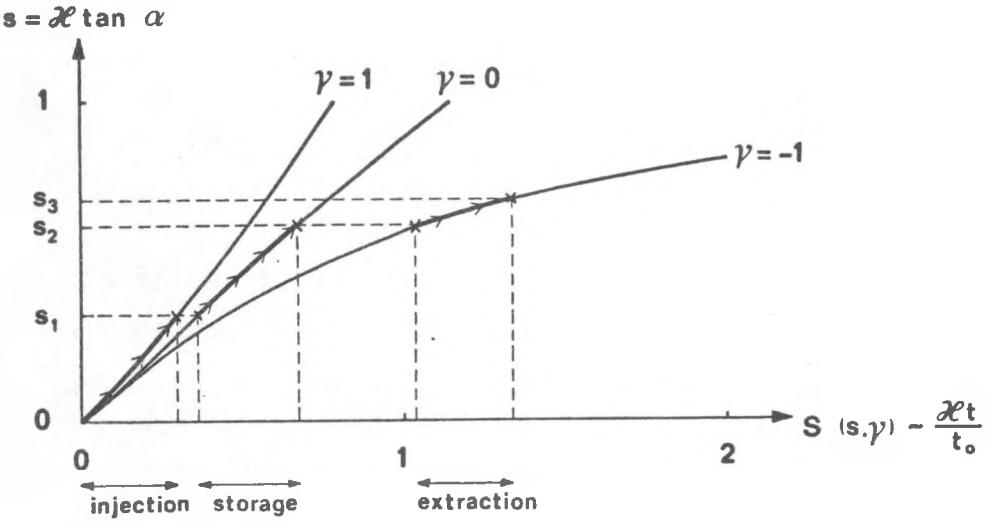

Figure 24. An example of tilting angle variation $\alpha(t)$ during a storage cycle.

We have an injection period with γ=1. Then there is a storage period with γ=0. During the extraction period we take γ=-1. Figure 24 shows the three curves $S(s,\gamma)$ from Figure 23. We start at t=0 with a vertical front: s=0. During the injection period we follow the curve S(s,1). The tilting s_1 at the end of the injection period is determined by the injection time. During the ensuing storage period we follow the curve S(s,0). We start from $s=s_1$. The tilting s_2 at the end of the storage period is obtained from the given storage time. During the subsequent extraction period we follow the curve S(s,-1). We start with the tilting s_2. The final tilting s_3 after injection, storage, and extraction is obtained from the given extraction time.

Figure 25 illustrates what may happen when we increase the injection, storage, and extraction periods.

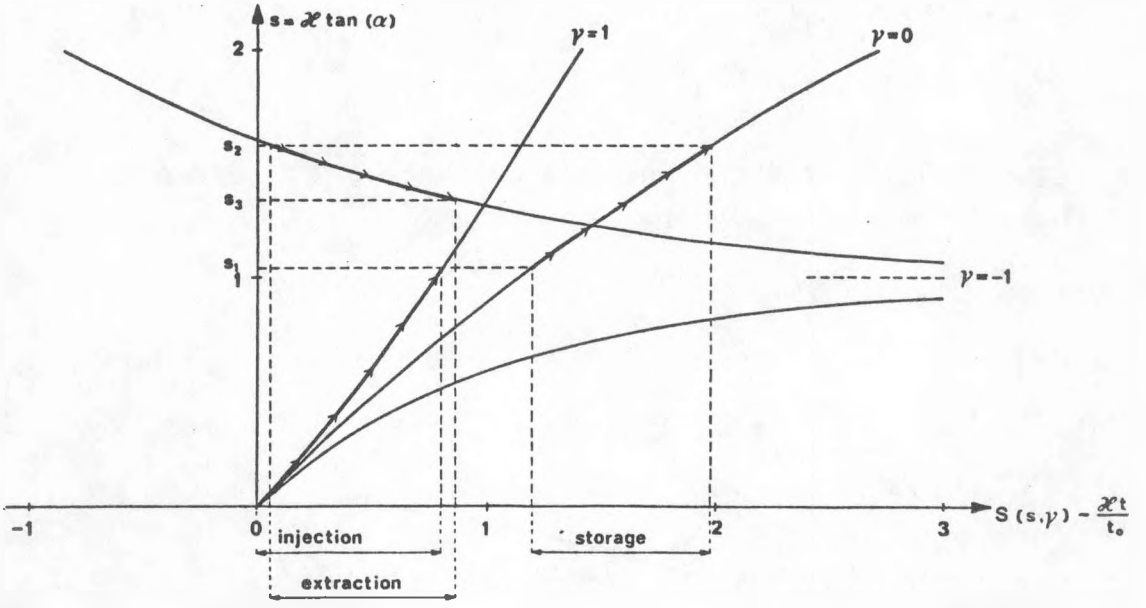

Figure 25. An example of tilting angle variation $\alpha(t)$ during a storage cycle.

The three curves $S(s,1)$, $S(s,0)$, and $S(s,-1)$ are again shown from Figure 23. The extraction curve $S(s,-1)$ has two branches. The tilting s_2 after the injection and storage periods is greater than $s=1$. So we must follow the upper branch of $S(s,-1)$.

The tilting angle increases during the extraction phase in our first example shown in Figure 24. It decreases in the second example of Figure 25, when the extraction starts with a tilting $s_2>1$. The tilting s moves toward the asymptotic value $-1/\gamma$ during the extraction phase. The upper decreasing branch is followed, when the initial tilting s_2 is greater than $-1/\gamma$. The increasing lower branch is followed, when the initial value s_2 is smaller than $-1/\gamma$. At the limit we have with the use of (76)

$$s = \kappa\tan(\alpha) = \frac{-1}{\gamma} = \frac{\kappa q_0 H}{-Q_1}\cdot\frac{\beta+1}{\beta-1} \qquad (84)$$

This is precisely the condition (54) for a stable front. The flow is horizontal and constant throughout the aquifer (48).

We will end this section with some explicit formulas for the tilting angle $\alpha(t)$. We assume that $0\leq s\leq 2$, $s=\kappa\tan(\alpha)$, so that (82) is valid.

Our first case concerns the pure buoyancy tilting of an initially vertical front. We have:

$$\gamma=0 \qquad \alpha(0) = 0 \tag{85}$$

From (75), (82), and (83) we get:

$$\tan(\alpha(t)) = \frac{1-e^{-f_1\kappa t/t_o}}{\kappa f_1} \qquad (\kappa\tan\alpha < 2) \tag{86}$$

Our next case concerns an injection period with a positive γ. The thermal front is again initially vertical:

$$\gamma>0, \qquad \alpha(0) = 0 \tag{87}$$

Then we have from (82) and (83):

$$\tan(\alpha(t)) = \frac{1}{\kappa} \cdot \frac{1-e^{-(\gamma+f_1)\kappa t/t_o}}{f_1+\gamma e^{-(\gamma+f_1)\kappa t/t_o}} \qquad (\kappa\tan(\alpha) < 2) \tag{88}$$

Tilting criterion for the injection period

The tilting of the thermal front during the injection period of the heat storage cycle is critical, since buoyancy and forced convection contribute cooperatively to the tilting rate. We can from the formulas of the preceding paragraph give a criterion which ensures a moderate tilting.

The formulas concerned a sharp front in a plane, infinite aquifer strip. Effects of the diffuseness of the front, of the finite distance to the injection well, and of cylindrical symmetry are not included.

Let the injection period be $0\leq t\leq t_i$. The thermal front is vertical at the beginning $\alpha(0) = 0$. Let γ_i be the injection parameter (76) for $Q_1=Q_i$. The tilting angle $\alpha_i=\alpha(t_i)$ at the end of the injection period is given by (88).

Let us require that the tilting angle α_i becomes smaller than 45^o. We have the criterion:

$$\alpha_i < 45^o \qquad \tan(\alpha_i) < 1 \tag{89}$$

We have with (88) the condition:

$$\frac{1}{\kappa} \cdot \frac{1-e^{-(\gamma_i+f_1)\kappa t_i/t_o}}{f_1+\gamma_i e^{-(\gamma_i+f_1)\kappa t_i/t_o}} < 1 \qquad (\kappa\tan(\alpha_i) < 2)$$

This may be rewritten to the following inequality:

$$\frac{t_i}{t_o} < \frac{1}{\kappa(f_1+\gamma_i)} \cdot \ln\left(\frac{1+\gamma_i\kappa}{1-f_1\kappa}\right) \qquad (\kappa<2) \qquad (90)$$

The criterion (90) ensures that the tilting angle α_i at the end of the injection period is less than 45^o. The characteristic tilting time is given by (27). The permeability ratio is $k'/k=\kappa^2$. We have that $f_1=0.235$ (77). The injection parameter is given by (76) with $Q_1=Q_i$.

Figure 26 illustrates the criterion (90). The region below the curves gives a moderate tilting during the injection phase ($\alpha_i<45^o$).

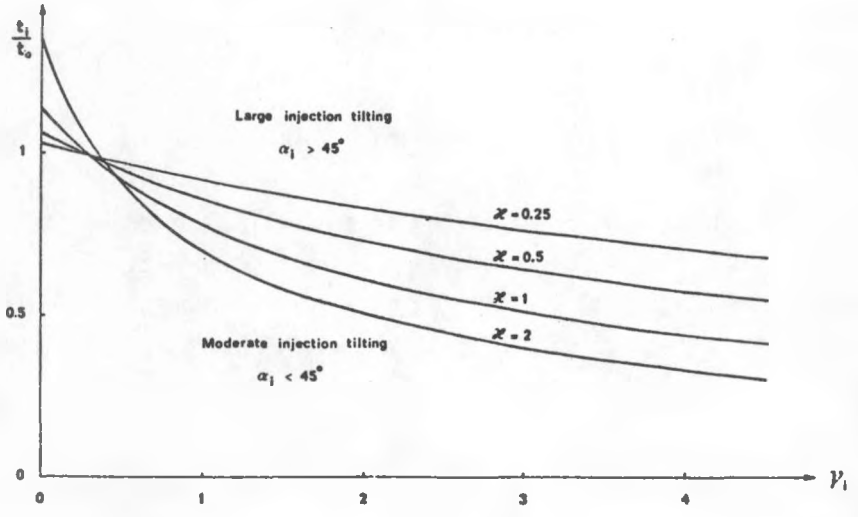

Figure 26. Injection tilting criterion (90) .

Let us illustrate criterion (90) in a more specific situation. We take:

$$\kappa = 1 \qquad t_i = 3 \text{ months} \qquad C_w/C = 1.5 \qquad (91)$$

Then we have from (29) and (77):

$$\frac{t_i}{t_o} = \frac{k}{H} \cdot A \qquad \gamma_i = \frac{Q_i}{kH} \cdot B$$

The coefficients A and B depend only on the temperatures T_0 and T_1. Formula (90) gives an inequality between k/H and $Q_i/(kH)$. The resulting curve for the limit with $\alpha_i=45^o$ is given in Figure 26' for four injection temperatures.

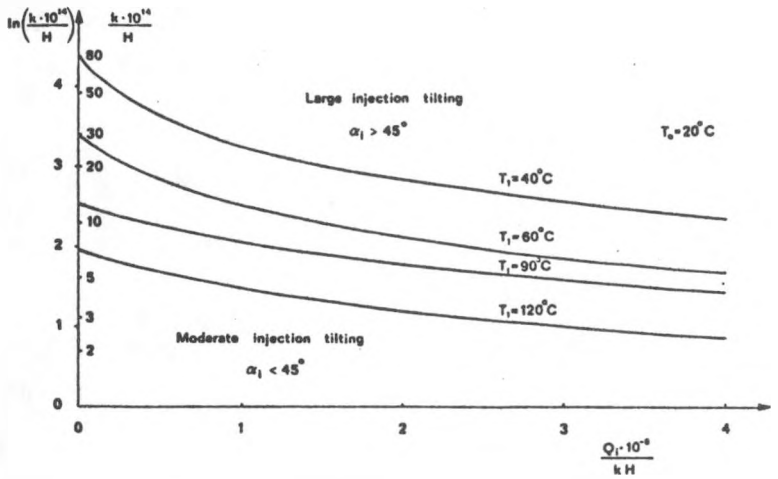

Figure 26'. The injection tilting criterion (90) in the special case of (91). The region below the curves gives an injection tilting $\alpha_i<45^o$.

Calculation of tilting angle

Formula (74) for the time development of the tilting angle concerns a sharp thermal front in an inifinite, plane aquifer. The previous analytical solutions for the buoyancy flow with a vertical thermal front included the additional effects of a diffuse thermal front, of a finite warm region, and of cylindrical symmetry. The influence of these three effects on the tilting rate is shown in Figure 16 and 17. We will in this section use these results to give an approximate formula for the tilting rate, when these three complications are taken into account.

Let us first discuss the modification of (74), when the diffuseness of the thermal front is considered. The temperature is T_1 on the warm side of the front and T_0 on the cold side. The temperature falls from T_1 to T_0 over the diffuse front. Let D denote the thickness of the front. This D is of course not a very precise quantity. It will increase with time due the heat diffusion: D=D(t). Dispersion effects for the flowing ground water may enhance the heat diffusion considerably.

Curve F in Figures 16-18 shows how the tilting rate is reduced, when the thickness D of the vertical thermal front increases. The dimensionless independent variable is $\kappa D/H$. Let us denote this function $f_D(\kappa D/H)$. It does not depend on the viscosity ratio. It is reasonable to assume that the buoyancy tilting is reduced approximately in the same way for a vertical and a tilted thermal front. The forced-convection contribution to (74) is kept unchanged. Formula (74) is now, when the diffuseness of the thermal front is taken into account in this approximate way, replaced by:

$$\frac{d}{dt}(\tan\alpha) = \frac{1}{t_o} f_t(\kappa\tan\alpha)\cdot\left[f_D(\frac{\kappa D}{H}) + \frac{Q_1}{q_o H}\cdot\frac{\beta-1}{\beta+1}\tan\alpha\right] \qquad (92)$$

The function $f_D(\kappa D/H)$ is given by curve F in Figure 16. The thickness of the thermal front D(t) is a given function of time.

We will use the one-dimensional solution for the heat diffusion in a case with an initially sharp temperature step. Let the temperature at the start t=0 be T_1 for $-\infty<x<0$ and T_o for $0<x<\infty$. The temperature T(x,t) is given by the complementary error function erfc:

$$T(x,t) = T_o + \frac{T_1-T_o}{2}\,\mathrm{erfc}(\frac{x}{\sqrt{4\lambda t/C}}) \qquad (93)$$

The thermal conductivity λ may have a considerable contribution from the dispersion that is associated with the ground water flow. Let λ_o be the thermal conductivity in the aquifer, when the ground water is at rest. The total thermal conductivity may be written:

$$\lambda = \lambda_o + \ell\cdot v_T C \qquad (94)$$

We are here only presenting a simplified description of the complicated dispersion phenomenon. The absolute value of the thermal displacement velocity is $v_T = qC_w/C$. The dispersion is characterized by the parameter ℓ. It has the dimension of a length. In a homogeneous aquifer ℓ is of the order of the grain size. In an inhomogeneous aquifer there is a macrodispersion. The length ℓ of (94) is then associated with the linear distances and dimensions of the inhomogeneities.

It is clear from character of the argument of erfc in (93) that the thermal zone width D increases as $\sqrt{4\lambda t/C}$. We have taken:

$$D = \sqrt{\frac{16}{\pi}}\cdot\sqrt{\frac{4\lambda t}{C}} \qquad (95)$$

The thermal conductivity is obtained from (94). A suitable mean value for v_T at the thermal front is used. The value of λ changes when v_T is changed. In such a case we take as a generalization of (95):

$$D(t) = \sqrt{D_o^2 + \frac{64}{\pi C} \cdot \int_o^t \lambda(t')\, dt'} \qquad (96)$$

Here D_o is the thickness of the thermal front at the starting time t=0.

Our next modification concerns the effect of the finite thickness of the warm region. We will consider both the plane and the cylindrical case. Our previous analytical solutions gave the effect for a perfectly vertical front. See Figure 7 B and E.

The effect on the tilting rate is shown in Figures 16 and 17 for two values of the viscosity ratio β. Curve B refers to the plane case and curve E to the cylindrical one. The relative tilting rate is given as a function of $\kappa L/H$, where L is the thickness of the warm region. Let us denote this function $f_B(\kappa L/H, \beta)$.

Let Q(t) be the rate of injection of water. We define L in the plane case and in the cylindrical case in the following way:

$$\begin{aligned} L(t) &= L(0) + \int_o^t \frac{C_w \cdot Q(t')}{CH}\, dt' \qquad \text{(plane)} \\ L^2(t) &= L^2(0) + \frac{1}{\pi} \int_o^t \frac{C_w Q(t')}{CH}\, dt' \qquad \text{(cylindrical)} \end{aligned} \qquad (97)$$

In the linear case Q is the volumetric flow per unit width of the aquifer (m^3H_2O/ms). The distance L gives the width of the warm region, if the flow were perfectly horizontal. In the cylindrical case Q is the total injection rate (m^3H_2O/s). The lenth L(t) is then the radius of the warm cylindrical region around the injection well.

The reduction of the tilting rate because of the finite width L was given by the function $f_B(\kappa L/H, \beta)$ for the buoyancy flow of a vertical front. It is a reasonable first approximation to assume the same reduction in our more general case with a tilted thermal front of finite width.

We have now the following approximate expression for the tilting rate, when the effect of the boundary is considered:

$$\frac{d}{dt}(\tan\alpha) = \frac{1}{t_o} f_t(\kappa \tan\alpha) \left[f_D\left(\frac{\kappa D}{H}\right) + \frac{Q_1}{q_o H} \cdot \frac{\beta - 1}{\beta + 1} \tan\alpha \right] \cdot f_B\left(\frac{\kappa L}{H}, \beta\right) \qquad (98)$$

This is our final expression for the tilting rate.

The characteristic tilting time t_o is given by (27). The characteris-characteristic tilting flow q_o is defined by (9). The function f_D is given by curve F in Figure 16. The width of the thermal front D(t) is given by (94) to (96).. The function f_B is given by curve B (plane case) or curve E (cylindrical case) for two values of β in Figures 16-17. The length L is given by (97).

A numerical solution of (98) is simple. The integration is performed with small discrete time steps. The injection rate Q(t) is any prescribed function of time. It is zero during storage periods and negative during extraction periods. The computer code for the numerical solution of (98) is reported in [4].

Let us end this paragraph with an example. We take a plane aquifer with the following data:

$$H = 20\ m \qquad k = 1.0 \cdot 10^{-11}\ m^2 \qquad \kappa^2 = 1$$

$$C_w = 4.1 \cdot 10^6\ J/m^3K \qquad C = 2.5 \cdot 10^6 J/m^3K$$

$$T_o = 20^oC \qquad \rho_o = 997.8\ kg/m^3 \qquad \mu_o = 1.002 \cdot 10^{-3}\ kg/ms \qquad (99)$$

$$T_1 = 90^oC \qquad \rho_1 = 965.6\ kg/m^3 \qquad \mu_1 = 0.3113 \cdot 10^{-3}\ kg/ms$$

$$\lambda = 1.5\ J/msK \qquad \ell = 0.6\ m$$

We consider an injection period t_i with an injection rate Q_1 followed by a storage period of the same length:

$$t_i = 10^6\ s = 11.6\ days$$

$$Q_i = 0.2 \cdot 10^{-3}\ m^3H_2O/ms$$

The characteristic buoyancy flow and the characteristic tilting time become:

$$q_o = 2.41 \cdot 10^{-6}\ m/s \qquad t_o = 19.7\ days$$

The distance L after the injection period becomes (97):

$$L(t_i) = 15.8\ m$$

The forced-convection tilting parameter becomes:

$$\gamma = 2.18$$

Figure 27 shows the time development of the tilting angle α under different assumptions.

Let us first consider the pure buoyancy flow of an initially vertical thermal front during a period t_i. Curve A shows the result for a sharp thermal front. Formula (74) with $Q_1=0$ has been used. Curve B shows the same process, when the effect of the diffuseness of the thermal front is included. Formula (92) with $Q_1=0$ has been used.

The curves C-F show the tilting angle during the injection and storage periods. The curve C is computed without the modifications for a diffuse front and a left boundary. Formula (74) has been used during the injection and storage periods. The curve D includes the boundary modification. Formula (98) with $f_D=1$ has been used. The curve E shows the tilting when the effect of the diffuseness is included. Formula (92) has been used. Finally, the curve F shows the result when both modification are considered The full formula (98) has been used.

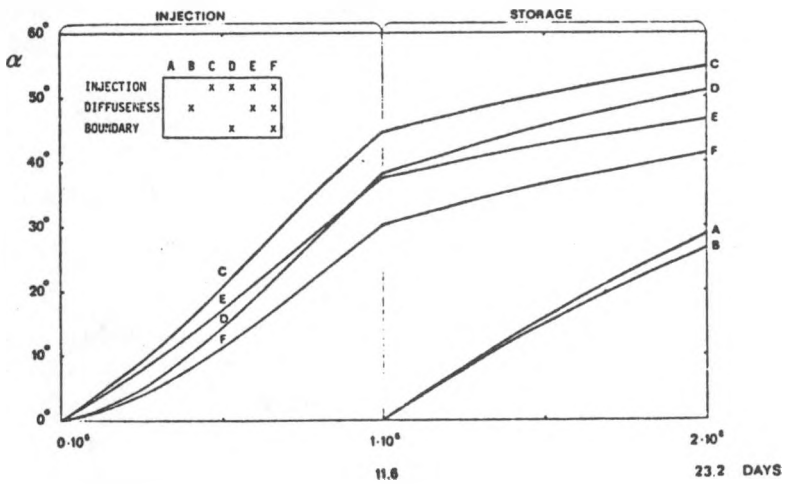

Figure 27. Tilting angle variation for the example of (99). The curves A-F refer to different assumptions.

The correction for the left boundary is illustrated if we compare C with D and F. There is a clear effect in the beginning, when $\kappa L/H$ is small. The effect is negligible when $\kappa L/H$ exceeds say 0.5.

The effect of the diffuseness of the thermal front is illustrated, when we compare A with B and C with E. The difference is considerably greater for the latter case. This is due the dispersion assumption (94). We had in case A and B:

$$v_T = 0 \qquad \lambda = 1.5 \text{ J/msK}$$

In case C-F we took during the injection phase:

$$v_T = \frac{4.1 \cdot 10^6}{2.5 \cdot 10^6} \cdot \frac{0.2 \cdot 10^{-3}}{20} = 1.64 \cdot 10^{-5} \text{ m/s}$$

$$\lambda = 1.5 + 0.6 \cdot 1.64 \cdot 10^{-5} \cdot 2.5 \cdot 10^6 = 26 \text{ J/msK}$$

Comparison with computer simulations

The main objective of this chapter is to study the validity of the assumptions made when deriving the analytical expression for the tilting rate (98). The following major assumptions were made.

a) Compressibility effects are negligible .

b) The curved thermal front is approximated by an appropriate straight line.

c) The diffuse front is represented by a zone with linearly varying density.

d) The analytical corrections for a diffuse front and for the effect of the well close to the front are valid even when the front is non-vertical.

e) The diffuse front does not reduce the forced-convection tilting rate.

A suitable way to test these assumptions is to utilize a numerical model of the aquifer system. The simulations have been performed with the computer code CCC developed at Lawrence Berkeley Laboratory. This code which encompares conduction, convection and compaction has been validated against a number of semi-analytic solutions and against the Auburn field experiment [5], [6] . The computer time expended to

simulate this problem puts some restrictions on the mesh size used in the numerical model. The treatment of the transport equation using finite difference methods (or finite element methods) introduces a spurious increase of the diffusion process. The character of the numerical dispersion tensor is such that it may be used to account for the effects of macroscopic dispersion [7]. In our simulations this numerical dispersion is equal to an additional thermal conductivity of about 15.0 J/msK during the injection period.

The simulations are performed with the following basic data for the plane aquifer:

Density of the solid	$2.5 \cdot 10^3$ kg/m^3
Specific heat of the solid	$0.9 \cdot 10^3$ J/kg
Thermal conductivity of solid-liquid mixture	1.5 J/msK
Specific storage of the porous media	$0.5 \cdot 10^{-4}$ m^2/N
Thermal expansivity of water	$0.317 \cdot 10^{-3}$ K^{-1}
Specific heat of water	$4.1 \cdot 10^3$ J/kg
Height of aquifer	20 m
Porosity	0.25

In the reference case we use:

Mass injection rate	0.2 kg/ms
Injection temperature	$T_1 = 90^oC$
Ambient temperature	$T_o = 5^oC$
Permeability	$k = 1.548 \cdot 10^{-11}$ m^2
Permeability ratio	$\kappa^2 = 1.0$
Injection period	$6.5 \cdot 10^5$ s ≈ 7.5 days
Storage period	$6.5 \cdot 10^5$ s ≈ 7.5 days

The aquifer is penetrated by three wells. Two wells are situated on opposite sides of a central well. The system is symmetrical with respect to a plane through the central well. This means that we only have to consider one half of the system. The distance between the wells is 300 meters.

Figure 28 shows the computed temperature field when the high permeability value $k = 1.548 \cdot 10^{-10}$ m^2 has been used. The temperature fields at the end of the injection period (Figure 28a) and at the end of the storage period (Figure 28b) are given.

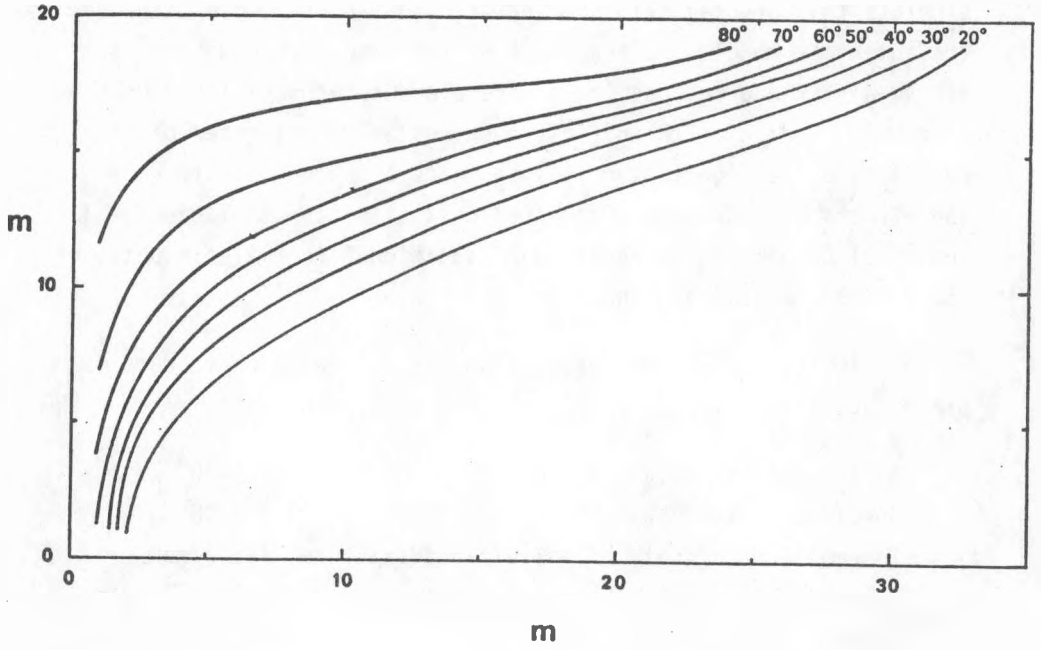

Figure 28a. Temperature field at the end of the injection period (7.5 days). The permeability is $1.548 \cdot 10^{-10}$ m^2.

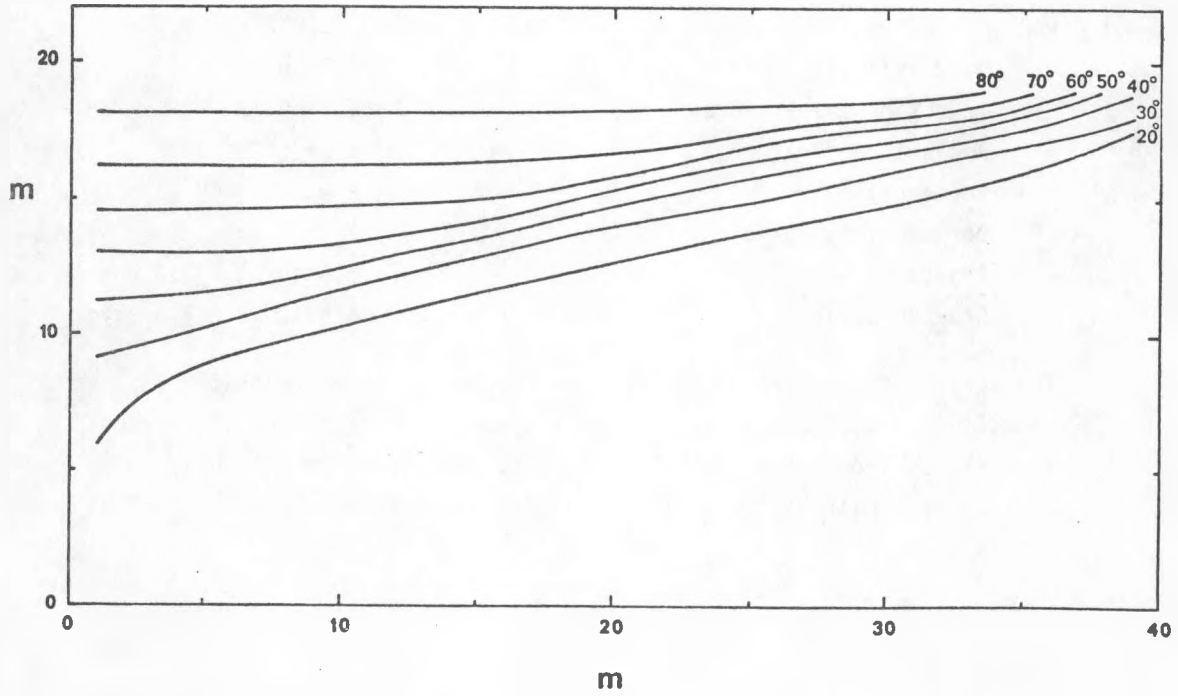

Figure 28b. Temperature field at the end of the storage period (15 days). The permeability is $1.548 \cdot 10^{-10}$ m^2.

The disadvantage of a very high permeability aquifer is clearly demonstrated. At the end of the storage period the hot water has been spread out in a thin layer adjacent to the upper confining stratum. Heat losses to confining layers are not included in the calculation. It is obvious that the heat losses from the aquifer would be substantially enhanced if the hot water behaves as in Figure 28.

When the permeability is ten times lower, $1.548 \cdot 10^{-11}$ m^2, the temperature fields are as shown in Figure 29. The tilting effects are still large considering the short period of time.

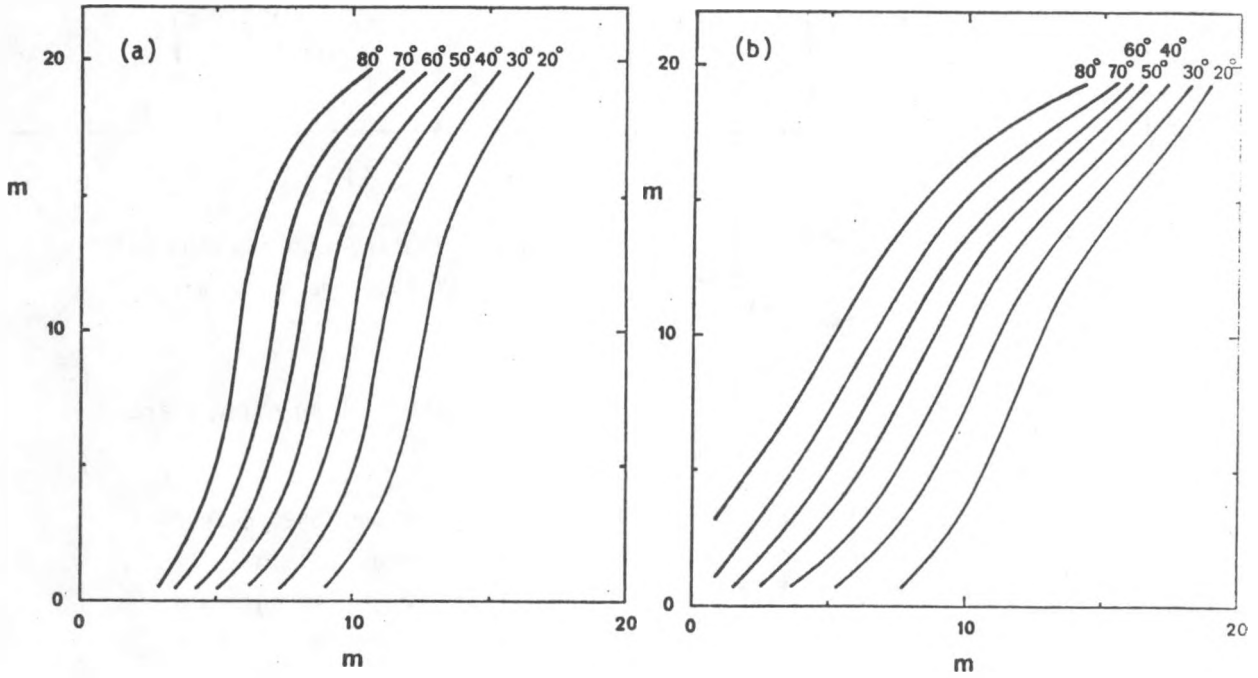

Figure 29. The temperature field at the end of the injection period (a) and at the end of the storage period (b). The permeability is $1.548 \cdot 10^{-11}$ m^2.

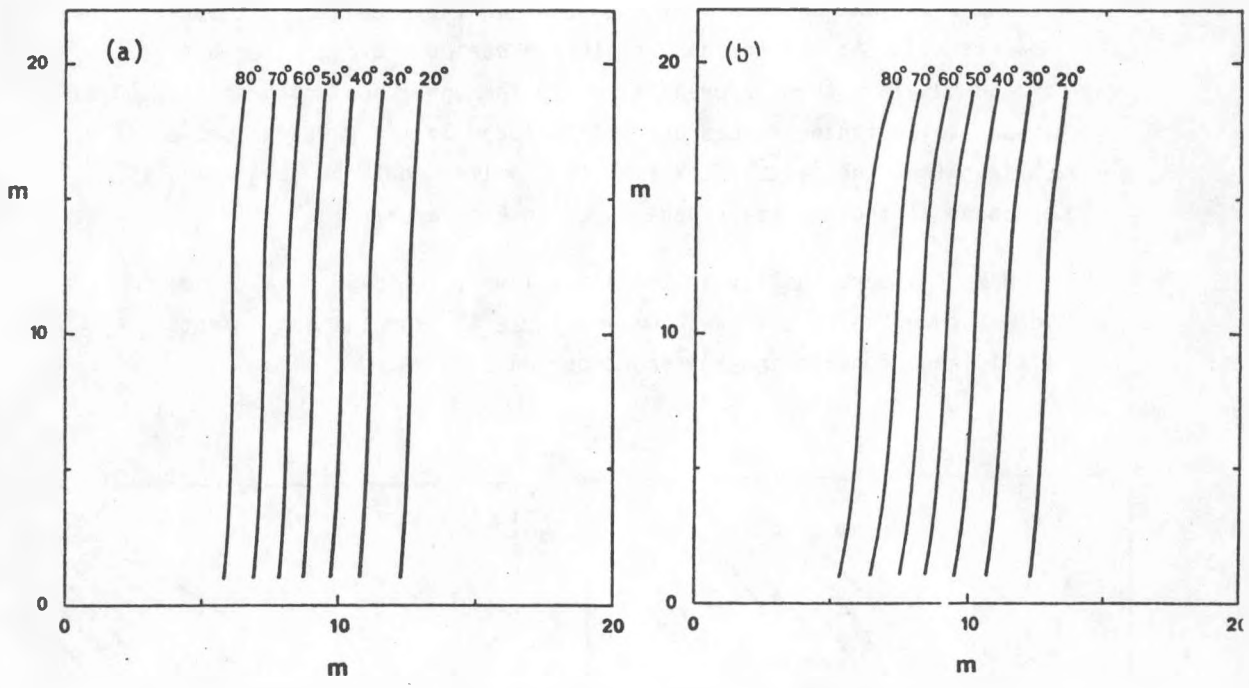

Figure 30. The temperature field at the end of the injection period (a) and at the end of the storage period (b). The permeability is $1.548 \cdot 10^{-12}$ m^2.

When the permeability is low, $1.548 \cdot 10^{-12}$, the tilting effects are small. See Figure 30.

The thermal front ($T = (T_1+T_0)/2 = 47.5^oC$) for the three different permeabilities are shown by the solid lines in Figure 31. The corresponding theoretical straight fronts are dashed. The agreement between the theoretical and the simulated thermal fronts is quite satisfactory.

Formula 29 indicates a strong dependence on the temperature levels of the injected and the ambient water. This effect is demonstrated in Figure 32. The tilting angle for the (60-20) case (degrees centigrade) is about one half of that for the (90-5) case. This is in agreement with theory. See Figure 15 where $\eta(60,20) = 2.62$ and $\eta(90,5) = 1.40$.

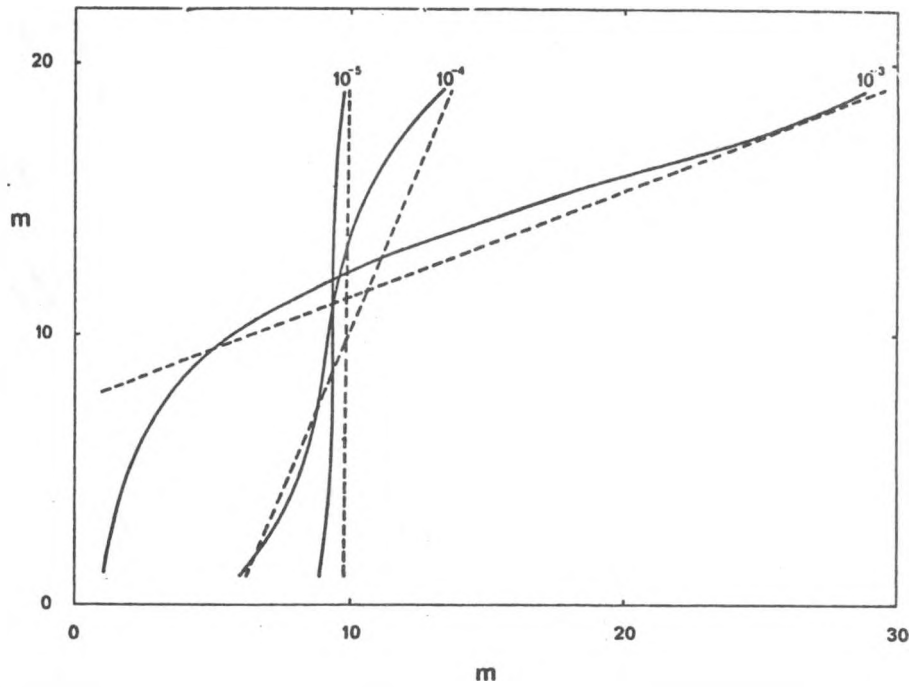

Figure 31a. The thermal fronts after the injection period (solid lines). The dashed lines give the corresponding theoretical ones. The hydraulic conductivity values 10^{-3}, 10^{-4} and 10^{-5} m/s ($T=5^{o}C$) correspond to the permeabilities $1.548 \cdot 10^{-10}$, $1.548 \cdot 10^{-11}$ and $1.548 \cdot 10^{-12}$ m^2 respectively.

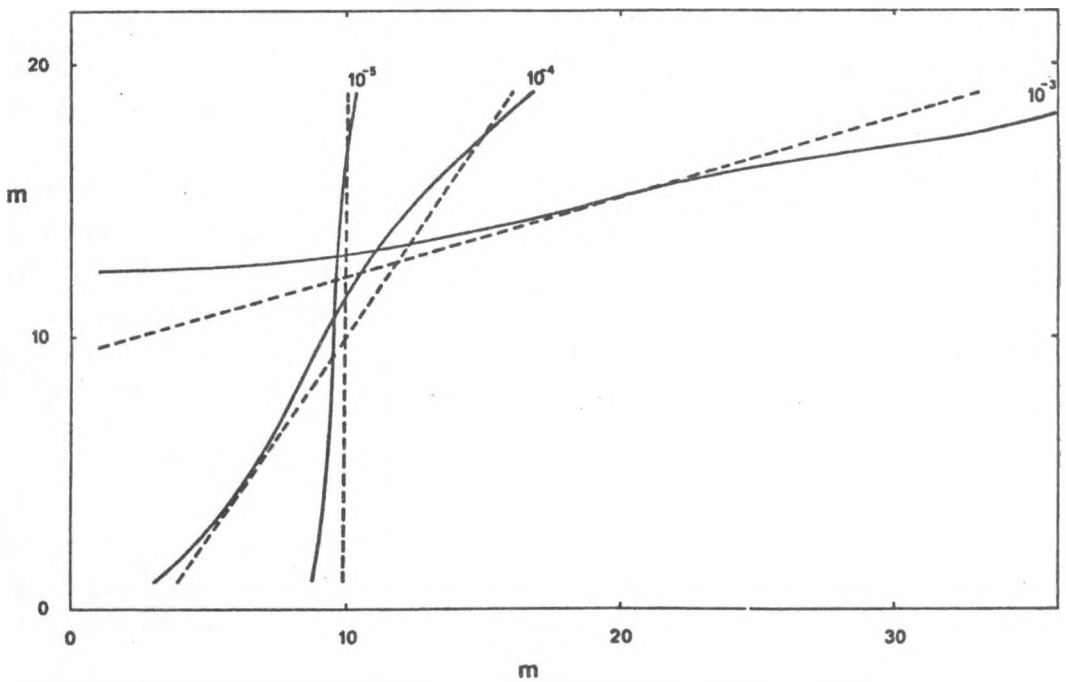

Figure 31b. The thermal fronts after the storage period (solid lines). The dashed lines give the corresponding theoretical ones.

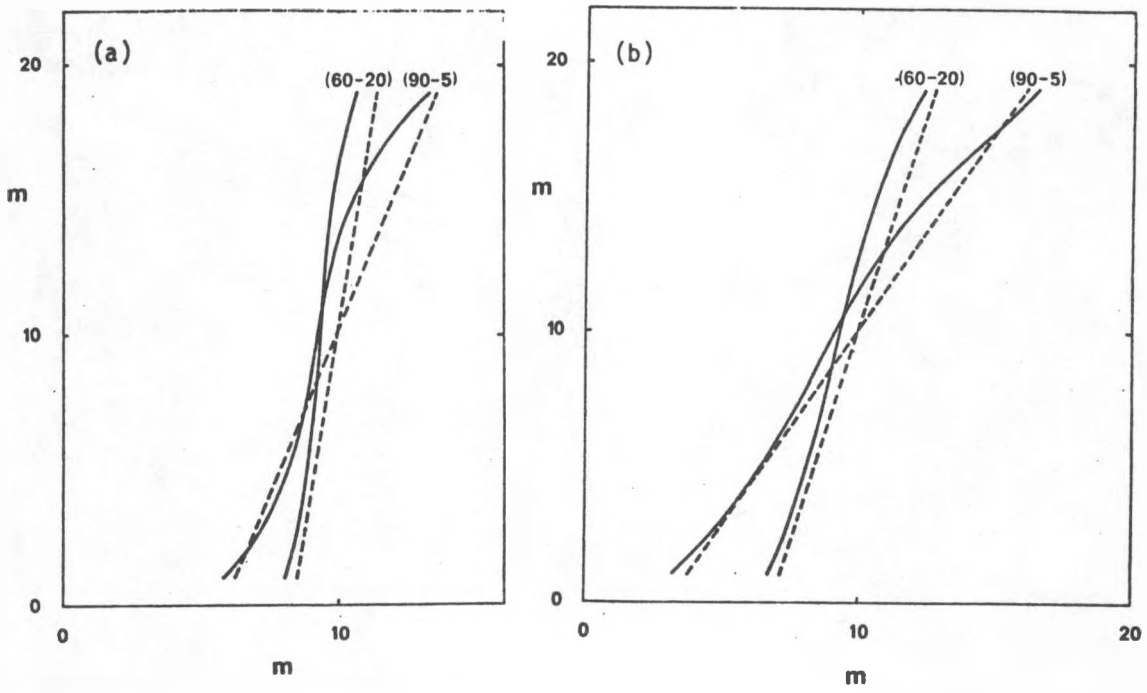

Figure 32. A comparison of thermal fronts after injection at different temperature levels. The simulated fronts (solid lines) and the theoretical fronts (dashed lines) are given at the end of the injection period (32a) and at the end of the storage period (32b).

The anisotropy of the permeability enters as the product $\kappa k = \sqrt{k'k}$ in the denominator of t_o (27). Thus, if κ is varied, while the quantity $\sqrt{k'k}$ is kept constant, the tilting time t_o will remain constant. In spite of this the tilting angle will not be the same. The reason is that both the correction for a diffuse front and that for a well close to the front have a κ-dependent parameter. There will be minor differences in the tilting angles if the anisotropy does not attain large values. Figure 33 shows the thermal front after the storage period for three different values of the anisotropy.

In the case $\kappa^2=0.1$ the thermal front retains the characteristic S-shape of a relatively sharp front. Compare with Figure 14. The reason for this is that the parameter $\kappa D/H$ is relatively small. In the figure both the simulated and the theoretical thermal fronts exhibit only small deviations from the isotropic case. But the relative positions of curve

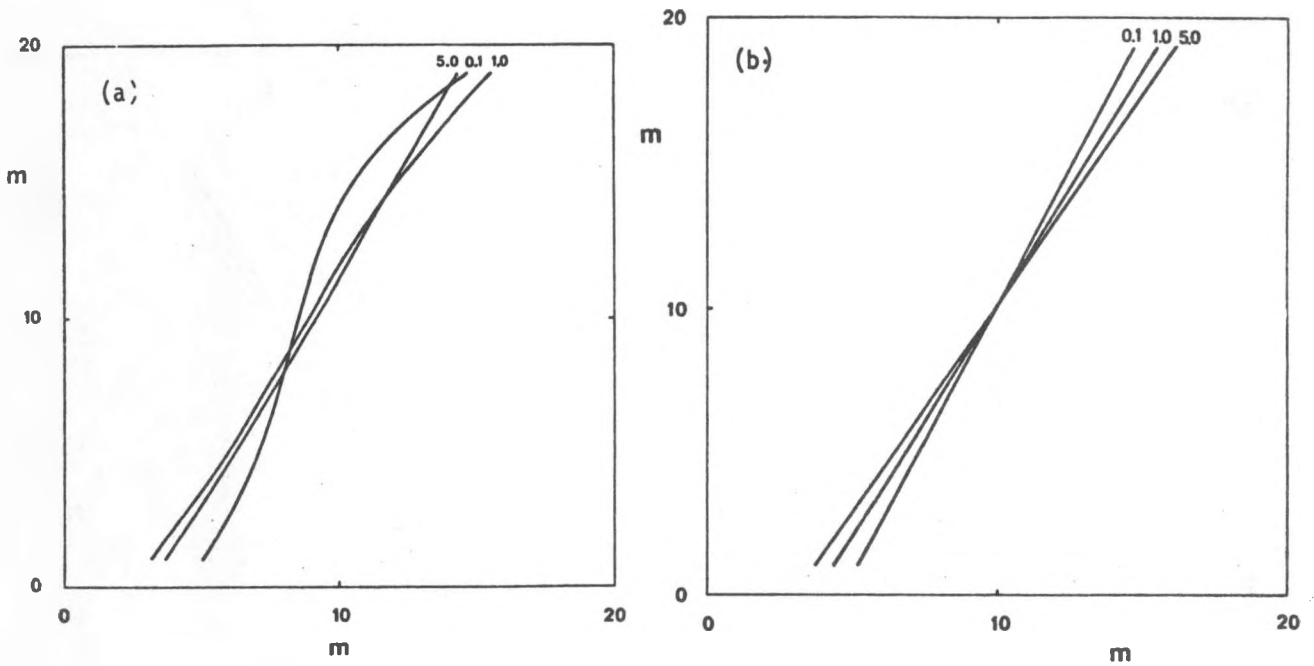

Figure 33. The simulated (a) and the theoretical (b) thermal fronts for different anisotropy (κ^2) values at the end of the storage period ($\sqrt{k'k}$ constant).

κ^2=5.0 is reversed. The difference is explained by the evaluation of the diffuse zone length. In the theoretical calculation the front was assumed to be sharp at the beginning and to evolve as the square root of time. The discrete representation of the temperature in the numerical scheme will give an initial diffuseness on the order of the width between the nodal points. At the start of the injection the diffuse zone will be too large. This reduces the flow.

Figure 34 shows the thermal front at the end of the storage period when the same volume has been injected with different flow rates. The length of the cycle, which consists of both the injection and storage periods, is kept constant. The flow rate of the reference case is denoted Q. The γ value corresponding to the flow rates 0.5Q, Q and 2Q is 1.14, 2.29 and 4.58 respectively.

It appears that, if the injection volume is given, the injection strategy is of little importance for the tilting angle at the end of the storage cycle. Compare with Figures 24 and 25.

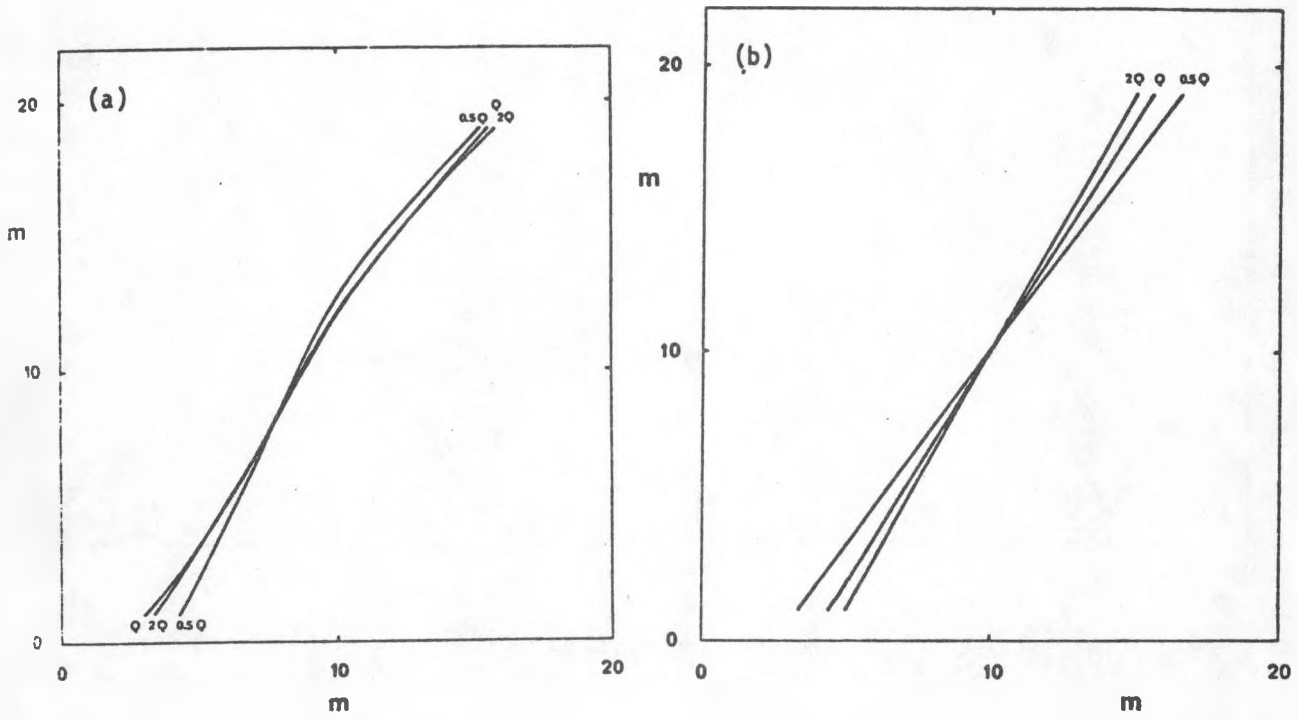

Figure 34. The simulated (a) and the theoretical (b) thermal fronts at the end of the storage period when the same volume has been injected at different flow rates. The length of the cycle, which consists of both the injection and the storage periods, is kept constant.

The general agreement between the simulated and the theoretical thermal fronts indicate that the assumptions made in the analytical approach are reasonable.

Discussion of field experiments

We shall in this section compare our theoretical results with some field experiments. These have been carried out at Neuchâtel (Switzerland) [8], Campuget (France) [1] and Auburn (USA) [9]. The basic data and the corresponding characteristic tilting time t_0 are given in Table III. The principal parameters are the height (H) and the permeability (k) of the aquifer, and the temperature of the injected (T_1) and the ambient water (T_0). The development of the tilting angle during the injection, storage, and production periods is calculated as previously described (98). The vertical permeability k' is often uncertain. The two values k'=k and k'=k/10 have been used in these cases. A thermal conductivity

	T_1(°C)	T_o(°C)	K(m/s)	k(m^2)	κ^2	H(m)	V_{inj}(m^3)	(days) t_{inj}	(days) t_{stor}	(days) t_{prod}	(days) t_o
Neuchâtel	51	11	$0.3\text{-}1\cdot10^{-2}$	$0.4\text{-}1.3\cdot10^{-9}$	1	7.2	494	9.3	124	28	0.2-0.6
Campuget	33.5	14	$1\cdot10^{-3}$	$1.15\cdot10^{-10}$	1	9	20,200	77	42+31	42+53	7.2
Auburn 1	36	20	$5\cdot10^{-4}$	$0.5\cdot10^{-10}$	0.1	10	8,000	3+10	10+36	26	55.6
Auburn 2	55	20	$5\cdot10^{-4}$	$0.5\cdot10^{-10}$	0.1	10	54,784	79	51	41	18.1
Auburn Ex	90	20	$5\cdot10^{-4}$	$0.5\cdot10^{-10}$	0.1	10	54,784	90	90	90	6.2
Low permeability aquifer	120	20	$1\cdot10^{-5}$	$1\cdot10^{-12}$	1	30	~90,000	90	90	90	166
Very low permeability aquifer	120	20	$1\cdot10^{-6}$	$1\cdot10^{-13}$	1	100	~90,000	90	90	90	5,530

Table III. Aquifer storage data and characteristic tilting time t_o.

of 1.5 or 15 J/msK has been used. The higher value represents a moderate macrodispersion. The step-wise computation of the tilting angle is discontinued, when $\alpha=60^{o}$ is attained. This is the limit for the simple approximation (73) of $f_t(s)$.

In the experiment at Neuchâtel (Switzerland) 494 m^3 of hot water at $51^{o}C$ was injected into an aquifer with a height of 7.2 meters. The aquifer consists of three layers with different permeabilities (400, 800 and 1300 Darcy). This gives a tilting time t_0=0.2-0.6 days. Figure 35 shows the computed variation of the tilting angle with time. In curve A we use the highest permeability value (1300 Darcy), a permeability ratio (κ^2) of 1.0, and a thermal conductivity (λ) of 1.5. This unfavourable case tilts to 60 degrees in just one day. If we instead use the lowest permeability, 400 Darcy, together with κ^2=0.1 and λ=15 J/msK, the tilting will reach the limit after 8 days. This should be compated to a storage period of 124 days. A strong disturbance of the temperature field due to buoyancy flow must be expected. This is in agreement with the field test.

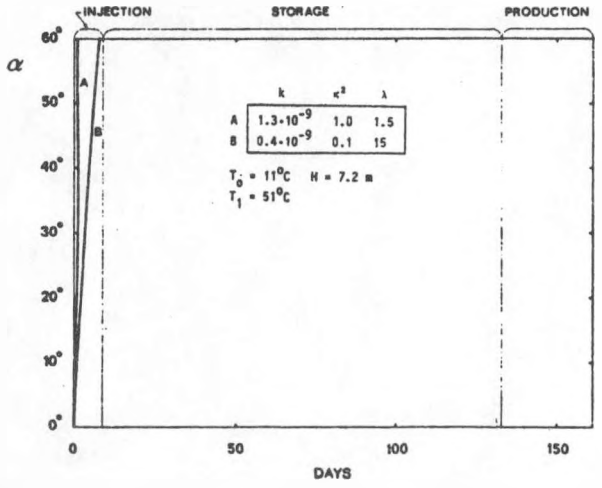

Figure 35. Neuchâtel. Theoretical tilting angle variation.

In Campuget (France) another field test was carried out during 1977-78 using an aquifer with a lower permeability (115 Darcy) and a height of 9 meters. The temperature difference was only 33.5-14^{o}C. This gives a characteristic tilting time t_0=7 days. The development of the tilting angle is given in Figure 36.

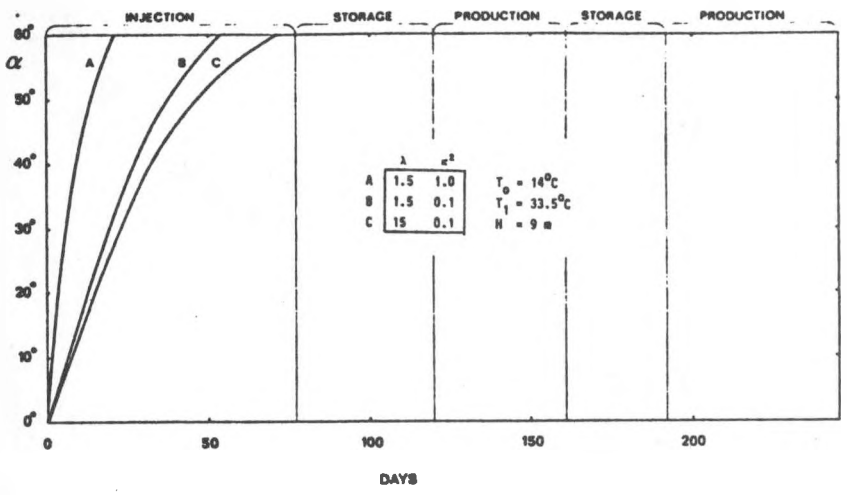

Figure 36. Campuget. Theoretical tilting angle variation.

The time to reach the 60 degrees limit varies from 21 days for case A to 71 days for case C. Since this is an alluvial aquifer, it is reasonable to assume that the vertical permeability is less than the horizontal one ($\kappa<1$). The whole storage cycle extends over 245 days. The calculations give a considerable tilting. A comparison with the field test is not simple. The situation is complicated by the large heat loss through the thin covering soil layer (1-3 meters). The effects of a strong buoyancy flow may then not be visible in the vertical temperatureprofiles but rather result in increased heat losses to the ground surface. The small fraction, 20%, of the injected energy that was recovered may support this interpretation.

The aquifer in the Auburn (Alabama, USA) field tests is located at a depth of 40 to 61 meters. The permeability is 50 Darcy. The well penetrates only the upper 9 meters of the aquifer. The calculations of a theoretical tilting angle are made with an aquifer height of H=10 meters.

During a numerical simulation of the first experiment if was necessary to assume an anisotropic permeabiltiy in order to get good agreement. The vertical permeability is set equal to 10% of the horizontal one. The result is that the tilting rate is reduced by a factor 3. In the first experiment the temperature difference was as low as 36 to 20°C. The tilting time t_0 is 56 days. The calculated tilting angles (Figure 37) reach values of 36° and 43° depending on the magnitude of the thermal

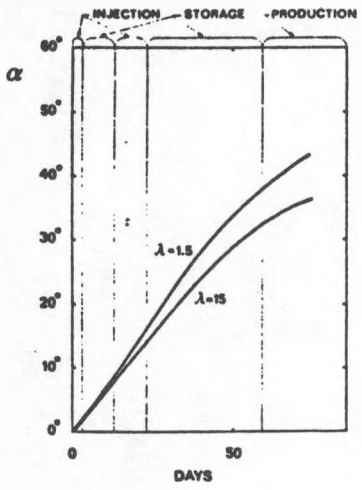

$T_0 = 20^oC$
$T_1 = 36^oC$
$H = 10$ m

Figure 37. Auburn 1. Theoretical tilting angle variation.

conductivity. In this case the calculations are stopped when the whole injected volume has been produced. The effects of the tilting should be rather limited during the a cycle of 85 days. The experimental temperature field indicates a tilting angle of 20^o at the end of the storage period. From Figure 37 we get a value around 35^o. The assumption that the lower part does not take part in the tilting process may account for this discrepancy. The presence of a cold water volume below the injected warm water will allow a closed streamline to extend into the lower region. The streamline will then be longer, and the flow will experience an additional flow resistance. See (7) and (8). The cold aquifer region below the heated volume will have a moderating influence on the tilting rate.

The first cycle of a second experiment was completed during 1978. The temperature of the injected water was now 55^oC. Due to this the characteristic tilting time t_o was lowered to 18 days. This illustrates the strong temperature dependence of the buoyancy flow. The increased buoyancy flow drives the tilting angle to 60^o in about 40 days. The experimental temperature field exhibits a pronounced tilting at the end of the storage period. The whole cycle is 175 days long. The theory over-estimates the tilting angle. This is due to the aforementioned intricacies of the partially penetrating well. Figure 38.

A wider field of applications of the aquifer heat storage concept can be found, if the water is stored at a higher temperature. In shallow aquifers a temperature of 90^o has been mentioned as desirable. Applied

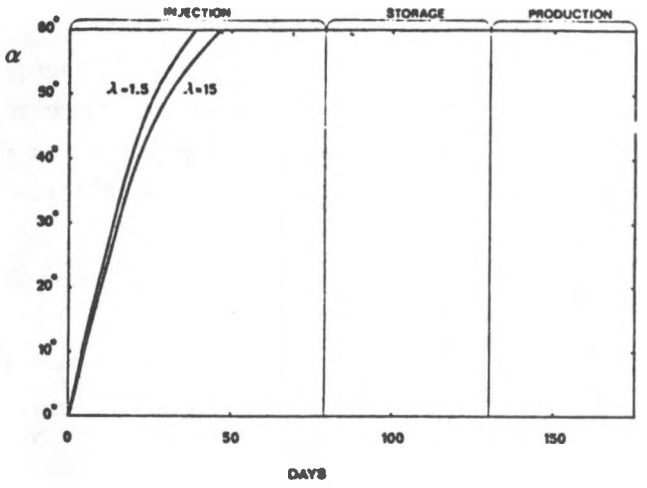

$T_o = 20^oC$
$T_1 = 55^oC$
$H = 10$ m

Figure 38. Auburn 2. Theoretical tilting angle variation.

at the Auburn test site this would give a characteristic tilting time t_o of 6 days. The buoyancy flow is then roughly ten times as high as in the first field test, where the injection temperature was 36^oC. Compare Figures 37 and 39. Annual storage means a longer storage cycle. The problem of thermal stratification then becomes further aggravated.

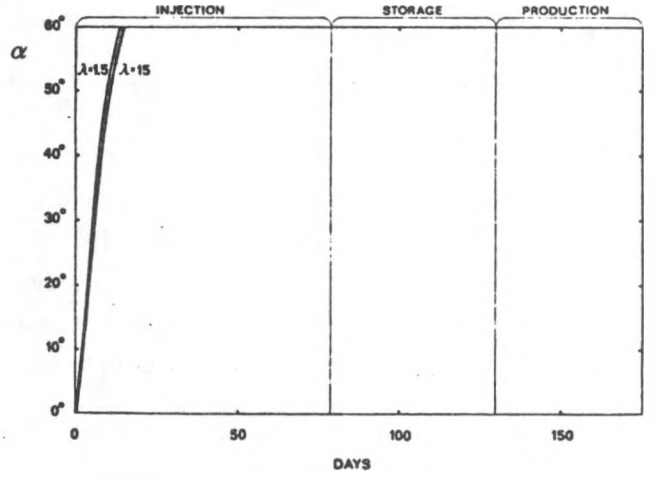

$T_o = 20^oC$
$T_1 = 90^oC$
$H = 10$ m

Figure 39. Auburn, Example. Theoretical tilting angle variation.

All the field tests conducted so far have utilized aquifers with rather high permeabilities and injected water of rather low temperatures. In the light of this investigation one must issue a warning for the substantial increase of the tilting flow that will

occur when larger temperature differences are used during longer storage cycles. An example of a promising system is given in Figure 40. The curves A-C show the tilting angle during a storage cycle for a low permeability system ($k=1\cdot10^{-12}$ m^2). Tight aquifers with this

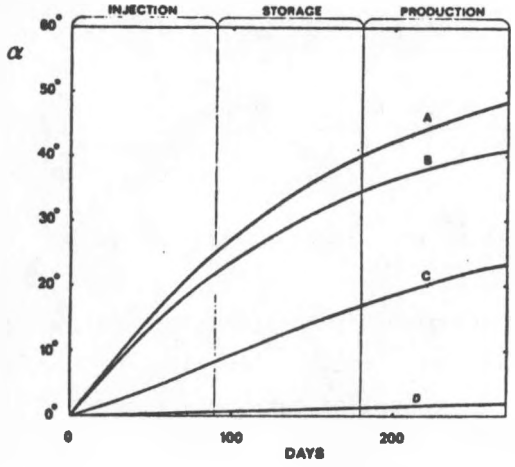

$T_0 = 20^oC$ $T_1 = 120^oC$

	k	κ^2	λ	H
A	$1\cdot10^{-12}$	1.0	1.5	30
B	$1\cdot10^{-12}$	1.0	7.5	30
C	$1\cdot10^{-12}$	0.1	1.5	30
D	$1\cdot10^{-13}$	1.0	1.5	100

Figure 40. Theoretical tilting angle variations for low permeability aquifers.

permeability can be found deeper down where it is possible to keep the water under pressure. Injection temperatures exceeding 100°C can then be utilized. As can be seen in Figure 40 the tilting rate is not large. The numerical simulation performed with the computer code CCC in 1976 used the same parameters as those resulting in curve D [5]. The corresponding tilting time-constant is 15 years. The buoyancy effects in this system is negligible as far as annual storage is concerned. This, together with the computed high efficiencies, points to the excellent performance of this kind of system.

The tilting is a major factor for the thermal performance of an aquifer heat storage system. We have seen that the tilting rate varies with as much as 10 000 times between different aquifers which have been studied or proposed. Great differences in thermal performance are to be expected. The extrapolation of the efficiency of a certain system to other cases must be made with great care and caution.

Conclusions

The two basic parameters for the tilting rate of the thermal front is the characteristic tilting time t_o (27) and the injection/extraction parameter γ (76).

The angular tilting rate of a sharp, vertical thermal front in a long, plane aquifer strip is $1/t_o$. This tilting rate is inversely proportional to the height H of the aquifer. It is proportional to the permeability $\kappa k = \sqrt{k'k}$. The buoyancy tilting rate depends strongly on the injection temperature T_1 and the ambient aquifer temperature T_o. The rate is increased 5 times, if we go from $T_o=10^oC$ and $T_1=40^oC$ to $T_o=10^oC$ and $T_1=90^oC$.

Let L denote the distance from the well to the vertical thermal front. The influence on the buoyancy tilting from the boundary of the well is negligible if $\kappa L/H>0.5$. This applies both to the plane and the cylindrical case.

The diffuseness of the thermal front diminishes the tilting rate. Let D be an appropriate width of the front. The tilting rate is reduced by 50%, when D increases from D=0 to $\kappa D/H=1$.

The effect of vertical anisotropy in the aquifer on the tilting is simple to assess. One shall use an effective permeability $\sqrt{kk'}$. If, for example, the vertical permeability is changed from k'=k to k'=k/10, then the tilting is reduced with the factor $\sqrt{1/10}\cong 0.3$.

The tilting angle increases during the injection and storage periods. It may increase or decrease during the extraction period. See Figures 24 and 25. The injection period, when buoyancy and forced convection cooperate, is the most critical one. Criteria that ensure only moderate injection tilting are shown in Figures 26 and 26'.

It is not possible to give any simple criterion how to avoid detrimental tilting during a storage cycle. Keeping this in mind we give the following guide-line, which is an upper limit on the quantity k/H. We get from Figure 26' with $Q_1=0$ for interseasonal storage:

		Aquifer height H (m)		
		10	25	50
Injection temperature T_1 (^oC)	60	3	8	15
	90	1	3	6
	120	0.7	2	4

Table IV. Order of magnitude upper limit for aquifer permeability k or $\sqrt{kk'}$ (Darcy) in order to avoid large tilting.

These values refer to a sharp thermal front. The diffuseness caused by heat dispersion will permit higher permeabilities. This is in particular the case for thin aquifers, where the thickness of the thermal front may be of the same order as the height H. In an anisotropic aquifer Table IV gives an upper limit on $\sqrt{kk'}$.

An aquifer which satisfies the condition of Table IV is expected to have a very good thermal performance. An assessment of the thermal performance of aquifers with considerably higher permeabilities than those of Table IV will require a more elaborate investigation.

Summary

The basic equations for the thermohydraulic process in the aquifer are given by (2), (3), and (4). The ground water flow in the aquifer with its displacement and, in particular, its tilting of the thermal front may at each moment be regarded as a superposition of a buoyancy flow and a forced-convection flow. The buoyancy flow is at work all the time, while the forced convection takes place during periods of injection and extraction.

The pure buoyancy flow of a vertical thermal front is analysed. The character of the buoyancy flow with its driving density differences is illustrated by Formulas (6)-(8). The starting point of the analysis is some exact solutions for the ground water flow. The considered cases are shown in Figure 7 A-F. The flow across the vertical thermal front is given by (18)-(23). These flows determine the tilting rate of the front.

The most important case is the tilting rate of a sharp front in a plane, infinite aquifer, Figure 7A. The basic tilting time for this case is:

$$t_o = \frac{\eta HC}{\kappa k C_w} \cdot 1.2 \cdot 10^{-6} \qquad (29)$$

The quantity η is a function of the injection temperature T_1 and the ambient temperature T_o, Figure 15.

The influence of the boundary of the well and of a finite width of the thermal front is shown by Figures 16-17. The infinite aquifer case according to Figure 7A gives the tilting rate with good accuracy except for quite thin warm regions ($\kappa L/H<0.3$) and for quite thick thermal fronts ($\kappa D/H>0.3$).

A simple buoyancy tilting criterion or guide-line is given by (30)-(35).

The superposition of buoyancy and forced convection is defined by the equations (36)-(38). A detailed dimensional analysis is made for the case of a sharp, tilted thermal front in a plane, infinite aquifer strip. See Figure 19. The tilting flow Q_t may be written (42)-(46):

$$Q_t = q_o H \cdot f_{bt}(\alpha,\beta,\kappa) + Q_1 \cdot f_{ft}(\alpha,\beta,\kappa)$$

The characteristic buoyancy flow q_o is defined by (9). The two functions f_{bt} and f_{ft} for the buoyancy tilting and the forced-convection tilting respectively depend only on the tilting angle α, the viscosity ratio $\beta=\mu_o/\mu_1$, and the anisotropy parameter κ (17). The time development of the tilting angle is given by (43):

$$\frac{d}{dt}(\tan\alpha) = \frac{8C_w}{H^2 C} Q_t \qquad (43)$$

There exists a certain combination of tilting angle α and pumping rate Q_1 for which the flow in the aquifer is constant and horizontal (48):

$$\tan(\alpha) = -\frac{q_o H}{Q_1}\frac{\beta+1}{\beta-1} \qquad (54)$$

The physical situation, when this happens, is illustrated in Figure 20. The tilting rate is zero, when (54) is satisfied. From this we may deduce the relation (56) between $f_{bt}(\alpha,\beta,\kappa)$ and $f_{ft}(\alpha,\beta,\kappa)$.

The effect of anisotropy is analysed. It is possible to reduce such a case to an isotropic one. We have for example:

$$f_{ft}(\alpha,\beta,\kappa) = f_{ft}(\alpha',\beta,1) \tag{65}$$

$$\tan(\alpha') = \kappa\tan(\alpha) \tag{61}$$

The remaining unknown function $f_{ft}(\alpha,\beta,1)$ is computed numerically, Table 1. It is shown that we can express the results with a single function $f_t(s)$:

$$f_{ft}(\alpha,\beta,1) = \frac{4G}{\pi^2}\tan(\alpha)\,\frac{\beta-1}{\beta+1}\,f_t(\tan\alpha) \tag{71}$$

The basic tilting function $f_t(s)$ is given in Figure 22 and Table II.

The final formula for the tilting rate of a sharp,tilted front in an infinite, plane aquifer becomes:

$$\frac{ds}{dt} = \frac{\kappa}{t_o}\,f_t(s)(1+\gamma s) \tag{79}$$

$$s = \kappa\tan(\alpha) \tag{75}$$

$$\gamma = \frac{Q_1}{\kappa q_o H}\cdot\frac{\beta-1}{\beta+1} \tag{76}$$

The solution of (79) is simple. The tilting s will follow the curves in Figure 23. Two examples of the tilting angle variation $\alpha(t)$ during a storage cycle are given by Figures 24 and 25.

The injection period, when buoyancy and forced convection cooperate, is the most critical one. The tilting at the end of the injection period is less than 45^o if

$$\frac{t_i}{t_o} < \frac{1}{\kappa(f_1+\gamma_i)}\,\ln\left(\frac{1+\gamma_i\kappa}{1-f_1\kappa}\right) \tag{90}$$

The length of the injection period is t_i. The injection parameter is γ_i, and $f_1 = 0.235$. Condition (90) is shown in Figure 26.

A modification of the tilting formula (79), which accounts in an approximate way for the finite width of the thermal front and for the well boundary in the plane and cylindrical case, is derived:

$$\frac{d}{dt}(\tan\alpha) = \frac{1}{t_o}\,f_t(\kappa\tan\alpha)\left[f_D\left(\frac{\kappa D}{H}\right) + \frac{Q_1}{q_o H}\cdot\frac{\beta-1}{\beta+1}\,\tan\alpha\right]f_B\left(\frac{\kappa L}{H},\beta\right) \tag{98}$$

An expression for the thickness of the thermal front, D(t), is given by (96). The distance to the well boundary is L (97). The function f_D is given by curve F in Figure 16. The function f_B is given by curve B (plane case) or curve E (cylindrical case) for two viscosity ratios in the Figures 16 and 17.

The complete tilting angle formula and different simplifications of it are illustrated in a particular case. See (99) and Figure 27.

The theoretical formulas have been compared with computer simulations of the complete thermohydraulic process in the aquifer. A computer code, called CCC, which has been developed at Berkeley, was used. Results are shown in Figures 28-30. The thermal fronts after the injection period and after a subsequent storage period are shown in Figure 31 a and b. The corresponding theoretical straight fronts agree very well with the numerically simulated ones. The agreement is also quite good in other cases, when the temperature levels T_1 and T_o, the anisotropy κ^2, and the injection rate Q, are varied. See Figure 32, 33, and 34 respectively.

The field experiments, which have been carried out at Neuchâtel, Campuget, and Auburn, are discussed. Data for these experiments are summarized in Table III. The characteristic tilting time t_o is also given.

The variation of the tilting angle according to (98) has been computed with different assumptions for these experiments. See Figures 35, 36, 37, and 38. The tilting angle passes 60^o in all cases except Auburn 1. This is basically due to the small value of the characteristic tilting time t_o compared to the time of the storage cycle.

The effect of the injection temperature T_1 is illustrated by the three cases Auburn 1 ($T_1=36^o$), Auburn 2 ($T_1=55^o$), and Auburn Example ($T_1=90^o$). The tilting rate is tripled from $T_1=36^oC$ to $T_1=55^oC$ and again from $T_1=55^o$ to $T_1=90^oC$. See Figure III. This drastic effect on the tilting is shown in Figures 37-39.

The advantage of aquifers with lower permeability is discussed. We get for a certain aquifer with a low permeability (k=1 darcy) a characteristic tilting time $t_o=166$ days. See Table III. In an aquifer with very low permeability (k=0.1 darcy) the characteristic tilting time became $t_o=$ 20 years. The modest (k=1 darcy) and negligible (k=0.1 darcy) tilting during an annual injection, storage, and production cycle is shown in Figure 40.

A few conclusions end the paper.

References

1. Proceedings of Thermal Energy Storage in Aquifers Workshop, May 10-12, 1978, Lawrence Berkeley Laboratory, Berkeley, California.

2. Heat Storage in Natural Ground Water Basins, Report, April 1978, Sören Andersson et al., Scandinavian Engineering Corporation; National Swedish Board for Energy Source Development.

3. Claesson, J. Notes on Ground Water Thermohydraulics, Report, Dep. of Mathematical Physics, Lund, Sweden, December 1979.

4. Hellström, G. Computer Code for Tilting Rate Formula. Report, Dep. of Mathematical Physics, Lund, Sweden, December 1979.

5. Tsang, C.F., Lippmann, M.J., Goranson, C.B. and Witherspoon, P.A. Numerical Modeling of Cyclic Storage of Hot Water in Aquifers. Lawrence Berkeley Laboratory, LBL-5929, 1977.

6. Narasimhan, T.N. and Witherspoon, P.A. An Integrated Finite Difference Method for Analyzing Fluid Flow in Porous Media. Water Resources Research, Vol. 12, No. 1, February 1976.

7. Claesson, J. Entropy Analysis of Numerical Dispersion. Department of Mathematical Physics, Lund, Sweden.

8. Mathey, B. Development and Resorption of a Thermal Disturbance in a Phreatic Aquifer with Natural Convection. Journal of Hydrology, 34 (1977) 315-333.

9. Molz, F.J., Parr, A.D., Andersen, P.F., Lucido, V.D. and Warman, J.C. Thermal Energy Storage in Confined Aquifers. Water Resources Research Institute. Auburn University, Preprint 1979.

APPENDIX. ANALYTICAL SOLUTION FOR A SHARP, VERTICAL THERMAL FRONT IN AN INFINITE STRIP.

We will in this appendix derive the analytical expression for the pressure in case A, which is shown in figure 7 A. The aquifer lies in the region $-\infty < x < \infty, -\frac{H}{2} < z < \frac{H}{2}$. The thermal front lies at $x = 0, -\frac{H}{2} < z < \frac{H}{2}$.

Let $P(x, z)$ denote the pressure in the aquifer. The pressure shall satisfy:

$-\infty < x < 0, -\frac{H}{2} < z < \frac{H}{2}$:

$$\frac{\partial}{\partial x}\left(\frac{k}{\mu_1}\frac{\partial P}{\partial x}\right) + \frac{\partial}{\partial z}\left(\frac{k'}{\mu_1}\left(\frac{\partial P}{\partial z} + \rho_1 g\right)\right) = 0 \qquad \text{(A 1)}$$

$0 < x < \infty, -\frac{H}{2} < z < \frac{H}{2}$:

$$\frac{\partial}{\partial x}\left(\frac{k}{\mu_o}\frac{\partial P}{\partial x}\right) + \frac{\partial}{\partial z}\left(\frac{k'}{\mu_o}\left(\frac{\partial P}{\partial z} + \rho_o g\right)\right) = 0 \qquad \text{(A 2)}$$

The horizontal boundaries are impermeable:

$$\frac{\partial P}{\partial z} + \rho_1 g = 0 \qquad z = \pm\frac{H}{2}, \quad -\infty < x < 0$$

$$\frac{\partial P}{\partial z} + \rho_o g = 0 \qquad z = \pm\frac{H}{2}, \quad 0 < x < \infty \qquad \text{(A 3)}$$

Hydrostatic conditions shall prevail far away from the thermal front:

$$P \to -\rho_1 g z \qquad x \to -\infty$$

$$P \to -\rho_o g z \qquad x \to +\infty \qquad \text{(A 4)}$$

The pressure and normal flow are continuous at the thermal front:

$$P(-0,z) = P(+0,z) \qquad (A\ 5)$$

$$-\frac{H}{2} < z < \frac{H}{2}$$

$$-\frac{k}{\mu_1} \cdot \frac{\partial P}{\partial x}\Big|_{x=-0} = -\frac{k}{\mu_o} \cdot \frac{\partial P}{\partial x}\Big|_{x=+0} \qquad (A\ 6)$$

We start with the following expressions:

$x < 0$:

$$P(x,z) = -\rho_1 gz + \sum_{n=0}^{\infty} a_n u_n(x,z) \qquad (A\ 7)$$

$x > 0$:

$$P(x,z) = -\rho_o gz + \sum_{n=0}^{\infty} b_n u_n(x,z)$$

where

$$u_n(x,z) = \sin\frac{(2n+1)\pi z}{H} \cdot e^{-\frac{(2n+1)\pi\kappa|z|}{H}} \qquad (A\ 8)$$

It is not difficult to verify that these expressions satisfy A 1 - A 4 for any choice of the coefficients a_n and b_n. The coefficients are determined by the two remaining conditions A5 and A6:

$$a_n = -\frac{q_o H\mu_1}{k} \cdot \frac{4}{\pi^2} \cdot \frac{(-)^n}{(2n+1)^2} \qquad (A\ 9)$$

$$b_n = -\frac{\mu_o}{\mu_1} \cdot a_n$$

In particular we have for the flow across the thermal front:

$$q_f(z) = -\frac{k}{\mu_1} \cdot \frac{\partial P}{\partial x}\Big|_{x=-0} =$$

$$= \kappa q_o \cdot \frac{4}{\pi} \sum_{n=0}^{\infty} \frac{(-)^n}{2n+1} \cdot \sin \frac{(2n+1)\pi z}{H} \qquad (A\ 10)$$

The series may be expressed in the simpler way of formula (18).

Notations

C	volumetric aquifer heat capacity (solid+water)	($J/m^3\ ^oC$)
C_w	volumetric water heat capacity	($4.2 \cdot 10^6\ J/m^3\ ^oC$)
D	thickness of thermal front	(m)
f_B	curve B (plane case) or curve E (cylindrical case) in Figures 16-18	(-)
f_{bt}	buoyancy tilting function	(-)
f_D	curve F, Figure 16	(-)
f_{ft}	forced-convection tilting function	(-)
f_t	basic tilting function (71)	(-)
$f_1=0.235$		(-)
G	Catalan's constant	(-)
g	standard gravity	($9.81\ m/s^2$)
H	height of aquifer stratum	(m)
h	driving hydraulic head	(m/m)
k	permeability (horizontal direction)	(m^2)
k'	permeability (vertical direction)	(m^2)
L	thickness of warm aquifer region	(m)
	distance to well boundary (97)	(m)
ℓ	macro-dispersion length (99)	(m)
L_y	thermal displacement corresponding to a time t_y	(m)
P	pressure in the ground water	(Pa)
P_b	buoyancy flow pressure component	(Pa)
P_{fc}	forced-convection pressure component	(Pa)
Q_{bt}	buoyancy tilting flow	(m^3H_2O/ms)
Q_{ft}	forced-convection tilting flow	(m^3H_2O/ms)
Q_t	tilting flow	(m^2/s or m^3H_2O/ms)
Q_1, Q_i	pumping rate	(m^3H_2O/ms)
$\bar{q}$	volumetric ground water flow	(m/s or m^3H_2O/m^2, s)
q_f	buoyancy ground water flow across the thermal front	(m/s)

q_o	characteristic buoyancy flow (formula 9)	(m/s)
R	radius of circular disc aquifer	(m)
$S(s,\gamma)$	tilting integral (81), (82)	(-)
s	tilting variable (75)	(-)
T	temperature	(^oC)
T_o	temperature of colder region	(^oC)
T_1	temperature of warmer region	(^oC)
t	time	(s)
t_i	injection time	(s)
t_y	time period of storage cycle	(s)
$t_o = \frac{1}{\omega_o}$	characteristic tilting time	(s)
$\bar{v}_T = \frac{C_w}{C} \bar{q}$	thermal velocity	(m/s)
v_o	characteristic thermal velocity	(m/s)
x, y	horizontal Cartesian coordinates	(m)
z	vertical Cartesian coordinate	(m)
$\hat{z}$	unit vector in the upward direction	(-)
α	tilting angle of thermal front	
α'	modified tilting angle (61)	
α_i	tilting angle after injection period	
$\beta = \frac{\mu_o}{\mu_1}$	viscosity ratio	(-)
Γ	closed curve in the aquifer	
γ	pumping rate parameter (76)	(-)
η	tilting time function	(-)
$\kappa = \sqrt{\frac{k'}{k}}$	permeability ratio	(-)
λ	thermal conductivity in the aquifer	(J/ms ^oC)
μ	dynamic viscosity for water	(kg/ms)
μ_i	dynamic viscosity for water at temperature T_i	(kg/ms)
ρ	density of water	(kg/m^3)
ρ_i	density of water at temperature T_i	(kg/m^3)
ω_t	angular tilting rate	(s^{-1})

ω_o	characteristic tilting rate	(s^{-1})
$\nabla=(\frac{\partial}{\partial x},\frac{\partial}{\partial y},\frac{\partial}{\partial z})$	gradient operator	(m^{-1})